Quality Metrics Of Digitally Derived Imagery and Their Relation to Interpreter Performance: I. Preparation of a Large-Scale Database

Final

TECHNICAL REPORT

April 1982

James J. Burke, Ph.D.
Robin N. Strickland, Ph.D.

Optical Sciences Center
University of Arizona
Tucson, Arizona 85721

Subcontractor to
Department of Industrial Engineering and
Operations Research
Virginia Polytechnic Institute and State University
Blacksburg, Virginia 24061

Contract F49620-78-C-0055
U.S. Air Force Office of Scientific Research
Life Sciences Directorate
Bolling Air Force Base, D.C. 20332

Quality Metrics Of Digitally Derived Imagery and Their Relation to Interpreter Performance: I. Preparation of a Large-Scale Database

TECHNICAL REPORT
April 1982

James J. Burke, Ph.D.
Robin N. Strickland, Ph.D.

Optical Sciences Center
University of Arizona
Tucson, Arizona 85721

Subcontractor to
Department of Industrial Engineering and
Operations Research
Virginia Polytechnic Institute and State University
Blacksburg, Virginia 24061

Contract F49620-78-C-0055
U.S. Air Force Office of Scientific Research
Life Sciences Directorate
Bolling Air Force Base, D.C. 20332

Unclassified

SECURITY CLASSIFICATION OF THIS PAGE *(When Data Entered)*

REPORT DOCUMENTATION PAGE	READ INSTRUCTIONS BEFORE COMPLETING FORM
1. REPORT NUMBER: AFOSR-TR- 83-0995	2. GOVT ACCESSION NO.: AD-A135631
	3. RECIPIENT'S CATALOG NUMBER:
4. TITLE *(and Subtitle)*: QUALITY METRICS OF DIGITALLY DERIVED IMAGERY AND THEIR RELATION TO INTERPRETER PERFORMANCE: I. PREPARATION OF A LARGE-SCALE DATABASE	5. TYPE OF REPORT & PERIOD COVERED: FINAL REPORT 1 June 1978 - 30 Sept. 1983
	6. PERFORMING ORG. REPORT NUMBER:
7. AUTHOR(s): James J. Burke, Ph.D. Robin N. Strickland, Ph,D.	8. CONTRACT OR GRANT NUMBER(s): Contract F49620-78-C-0055
9. PERFORMING ORGANIZATION NAME AND ADDRESS: Dept. of Industrial Engineering and Operations Res. Virginia Polytechnic Institute and State University Blacksburg, Virginia 24061	10. PROGRAM ELEMENT, PROJECT, TASK AREA & WORK UNIT NUMBERS: 61102F 2313/A4
11. CONTROLLING OFFICE NAME AND ADDRESS: Air Force Office of Scientific Research (NL) Bolling Air Force Base, D.C. 20332	12. REPORT DATE: April 1, 1982 13. NUMBER OF PAGES: 104
14. MONITORING AGENCY NAME & ADDRESS *(if different from Controlling Office)*	15. SECURITY CLASS. *(of this report)*: Unclassified 15a. DECLASSIFICATION DOWNGRADING SCHEDULE

16 DISTRIBUTION STATEMENT *(of this Report)*

Approved for public release; distribution unlimited.

17. DISTRIBUTION STATEMENT *(of the abstract entered in Block 20, if different from Report)*

18. SUPPLEMENTARY NOTES

19 KEY WORDS *(Continue on reverse side if necessary and identify by block number)*

Image quality
Photointerpreter performance
Digital images
Digital processing

20 ABSTRACT *(Continue on reverse side if necessary and identify by block number)*

This report describes the preparation of an imagery database containing 250 transparencies, consisting of 25 degraded versions of each of 10 digitized images. The 25 degraded versions consist of 5 blur levels combined with 5 noise levels. Each image is 86 mm square and represents 4096 x 4096 8-bit pixels. These images have corresponding ground truth, and the blur and noise levels are verified and quantitatively known.

DD FORM 1 JAN 73 1473 EDITION OF 1 NOV 65 IS OBSOLETE

Unclassified

SECURITY CLASSIFICATION OF THIS PAGE *(When Data Entered)*

Subsequent stages of the research program will use these images in experiments to compare image quality with measured photointerpreter performance. An overview of the research program is also provided.

TABLE OF CONTENTS

LIST OF FIGURES

Figure

LIST OF TABLES

PREFACE

This research was supported by Contract No. F49260-78-C-0055 from the Air Force Office of Scientific Research, under the monitorship of Dr. Alfred R. Fregly. Dr. Harry L. Snyder is the principal investigator.

I. INTRODUCTION TO THE RESEARCH PROGRAM

It is appropriate to begin this first report of the series with an overview of the entire research program--its motivation, objectives, approach, and constraints. This will be followed by a summary discussion of the database, from its origin to its production on digital magnetic tape and in hardcopy display. Finally, detailed measures of the database occupy the bulk of this report.

STATEMENT OF THE PROBLEM

Recent technological developments have resulted in a wide variety of imaging systems and subsystems. The flexibility and technologies available to the designer include various means for collection, coding, transmitting, decoding, analog and digital processing, and analog and digital display. The applications of such systems and subsystems are myriad, ranging from static and dynamic military photointerpretive functions, through commercial and closed-circuit television and facsimile systems, to diagnostic radiological instrumentation and earth resources applications. The scientific world is quite familiar with some of the techniques which can be used to "improve" the nature of any such image, and the non-scientific world has equally seen

examples of processing effectiveness, such as the Zapruder and Hughes films of the Kennedy assassination. In many cases, it is clear that such processing and display techniques can extract information in the original image which is otherwise well below the threshold capacity of the human visual system, whereas in other cases it is clear that processing techniques can often serve either to hide existing, and important, image detail or to "create" image detail which is perhaps not present in the original image or in the "real world". Heretofore, most of these areas of image system and subsystem development have plainly suffered from their inattention to human observer requirements. This is particularly true of the extensive effort in digital image processing, especially that part devoted to the improvement ("enhancement", "restoration") of images for purposes of human information extraction. In nearly all of the work performed in laboratories around the country that are pursuing this type of research, the necessary evaluative efforts to determine the utility of processing and display techniques have not been conducted. Rather, reports and publications of this work typically take the form of "before and after" pairs of images, where the reader is left to estimate the utility of such images either by visual inspection of these published (second- or third-generation) photographs or by the subjective opinions offered in the text by the author.

Because the intent of such image processing techniques is to improve the information extraction capabilities of the human observer, it is clearly appropriate and mandatory that evaluative techniques include objective measurement of human information extraction from such images, rather than merely subjective estimates of the overall quality or utility of the image. Unfortunately, the human factors experiments required to produce quantitative and objective assessment of image quality have rarely been conducted in image processing laboratories or in conjunction with image processing programs.

In view of the many millions of dollars being devoted to image collection, processing, and display systems for the military and civilian use of digitized images, it is quite clear that an assessment program is urgently needed to devise procedures, techniques, and metrics of digital image quality. Such a program requires the establishment of a standardized set of procedures for obtaining human observer information extraction performance; relating this performance, in a quantitative manner, to the various collection, processing, and display techniques and algorithms; and devising a quantitative relationship for the multi-dimensional scaling of the various collection, processing, and display techniques in "performance space".

Only through such an integrated program of research can the system and subsystem designer have meaningful data for

cost-benefit analysis of future system development, be such systems intended either for military or for non-military applications. The image collection, processing, and display technology is now at a point whereby such evaluative research is sorely needed. Fortunately, microphotometric, microdensitometric, and human performance measurement techniques have been evolved during the past several years to relate human information extraction performance to the various physical characteristics of both electro-optical and photographic image displays. The present research program is designed to extend these recently developed techniques into the arena of digital images, emphasizing derivation of metrics of image quality appropriate to digitized images, and providing quantitative cost-benefit data which will permit the designer and system developer to plan his developmental effort as well as to specify optimum system components for particular image acquisition and display requirements.

OVERVIEW OF THE RESEARCH PLAN

The research plan is laid out schematically in Figure 1. Each small, solid-lined box, with the exception of the uppermost, indicates a separate task to be conducted during the course of the four-year effort. The two large, broken-lined boxes delineate the specific display formats that will be studied and compared during this initial program: black

and white hard copy transparencies and electronic displays. The small, broken-lined box at the bottom illustrates important extensions of this research to be pursued in the future, namely interactive digital displays in both black and white and in full color. The present report describes in detail the execution of the first two steps of this overall plan, specifically the creation of the database of known content and with controlled image degradation.

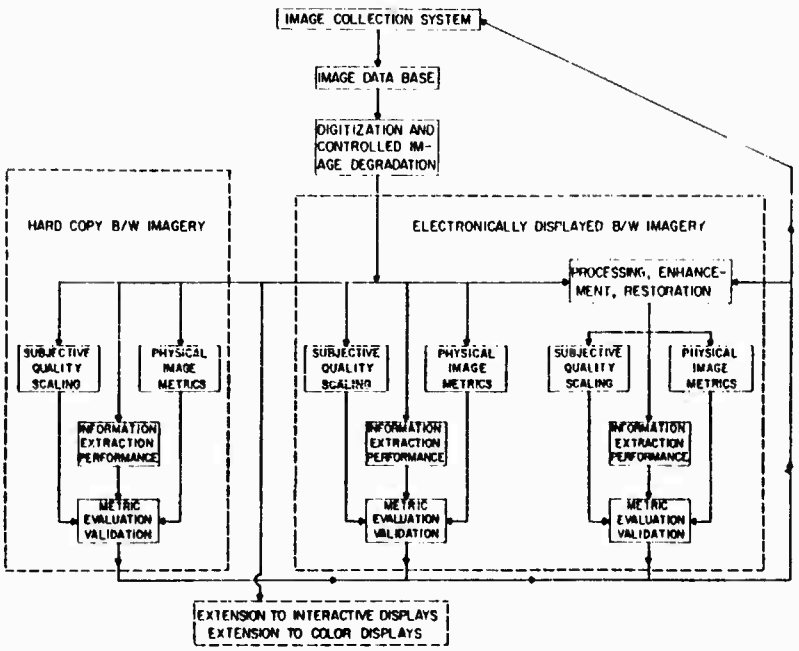

PROGRAM OVERVIEW

Figure 1: Schematic diagram of proposed research

Research Objectives

The research objectives of this program are as follows:

1. Develop standardized procedures and techniques to evaluate hard-copy (film) and soft-copy (CRT) digital image quality.

2. Compare candidate physical metrics of image quality.
3. Compare hard-copy with soft-copy displays for image interpretation.
4. Evaluate candidate processing, enhancement, and restoration algorithms for improvement of image interpretation on soft-copy displays.

Specific Research Tasks

In keeping with the general goals described above, the specific research tasks are as follows:

1. Develop an imagery database and image interpretation scenarios from high quality aerial photographs relevant to the image interpretation task.
2. Select and purchase display and interface hardware to present the image database on soft-copy (CRT) displays.
3. Develop image manipulation software for soft-copy and hard-copy experiments.
4. Develop and standardize observer data collection procedures for hard-copy and soft-copy experiments.
5. Develop and standardize procedures for obtaining physical image metrics from hard-copy and soft-copy displays.
6. Digitize and degrade database imagery and record images on hard copy and magnetic tapes for soft-copy display.

7. Obtain physical image metric data for hard-copy and soft-copy displays.
8. Conduct subjective quality scaling and information extraction studies on hard-copy images.
9. Conduct subjective quality scaling and information extraction studies on soft-copy displays.
10. Evaluate the utility of image quality metrics for both hard-copy and soft-copy imagery.
11. Conduct subjective quality scaling and information extraction studies on processed soft-copy imagery.
12. Analyze utility of image quality metrics for processed soft-copy imagery.
13. Compare image quality metrics for hard-copy and soft-copy (processed and nonprocessed) images. Relate these results to concepts and models of human visual performance and to imaging system variables.

Program Ground Rules

The overriding objective of this program is to provide a scientific contribution in the area of digital image quality and image metrics, which would be relevant to the field of military photointerpretation and, at the same time, be available to the scientific community. To be realistic and consistent with tactical interpretation scenarios, close coordination was maintained with Hq USAF, TAC, and RADC at critical stages of the research, in particular during imagery selection.

The degree of realism was also enhanced by using photointerpreters with experience relevant to the types of imagery employed. Thus, criteria for imagery selection included excellent quality and content typical of tactical scenarios.

Finally, all output from the program, including results and the imagery database, are unclassified and will be reported in the open literature. It is hoped that future investigations of digital image quality will use the same, available database to permit comparisons with and extensions of our results.

II. OVERVIEW OF DATABASE DEVELOPMENT

ORIGINAL MATERIAL AND PHOTOINTERPRETATION SCENARIOS

The original negative transparencies, from which our low-altitude aerial photographic database was generated, were acquired from the film libraries of the Environmental Research Institute of Michigan (ERIM). With the support and encouragement of sponsors of some of their prior research, Messrs. Robert Horvath and Stephen Stewart of ERIM aided us in locating promising candidate materials. These were taken to Langley AFB, Virginia, where we and personnel of the 460th Reconnaissance Technical Squadron, together with Dr. Harry Snyder, Dr. Michael Maddox, and Mr. James Turpin of VPI&SU, identified suitable 7.6 x 7.6 cm target areas and developed essential elements of information (EEIs) therein. Earlier visits to Langley AFB, arranged and accompanied by Mr. Gilbert Kuperman of AMRL, Wright-Patterson AFB, Ohio, had resulted in the full and enthusiastic cooperation of the Tactical Air Command. Their support and encouragement continues to be an essential contribution to the viability of our studies.

The original photographs were generated by a K17 camera, with a 74 degree FOV, W12 filter, 15.2 cm focal length, and 1/250 shutter speed, at f/11. Four are in Kodak Plus-X

Aerial Film 3401; the rest are in Kodak Tri-X Aerographic Film 2403. Of the 10 scenes used in our hardcopy studies, 4 cover U.S. airfields, 4 more cover U.S. naval installations, and 2 illustrate electronic and/or R D installations. Scales range from 1:2700 to 1:4400.

Also transported to Langley AFB on several occasions were hardcopy displays of digitally processed images, degraded by Gaussian blur and noise. These were prepared by Dr. Robin Strickland and Mr. Thomas Bruegge, employing the UA's CYBER 175 computer, the DEC 11/70 - IIS 70/E pipeline processor system in the Digital Image Analysis Laboratory (DIAL), and the Eclipse S/230-PDS microdensitometer in the Optical Sciences Center (OSC). The purpose of these early blurred and noisy images was to establish a meaningful range of these parameters for use in subsequent psychophysical studies. It was our intention to include material both better and worse than that typically encountered by tactical photointerpreters, with an adequate sampling of the parameter space between these extremes. Several iterations were required to obtain the desired range and sampling density.

We began with the idea of using image contrast as a third, independent, dimension. Discussions with senior interpreters indicated, however, that this was unnecessary, if not undesirable. Something more akin to a dimension measuring signal-to-noise ratio (SNR) was indicated.

Because all scenes contained targets of varying size and contrast, we adopted the maximum (peak) intensity as our definition of "signal", adding noise proportional to peak signal. All scenes were scanned to yield peak digital values of approximately 2000. Nominal SNRs of 200, 100, 50, 25, and 12.5 were selected for these studies.

INITIAL SELECTION OF EQUIPMENT AND MATERIALS FOR DIGITIZATION

Our plans called for the OSC Eclipse-S230/PDS-microdensitometer to serve as our primary facility for the generation of the large-scale (4096 x 4096) digital images on magnetic tape (digitization at 20 μm steps with Gaussian scanning apertures of 20, 40, 80, 160, and 320 μm full-width half maximum (FWHM)), digital noise addition, and hardcopy display (positive transparencies written on Kodak Technical Pan 2415 by the microdensitometer with 20 μm aperture and step size). The DIAL laboratory, on the other hand, would serve as the UA's principal facility for preparing and displaying softcopy images, in 512 x 512 format, during future studies of enhancement and restoration techniques. A similar but more extensive facility, composed of a DEC 11/55 with multiple disk drives and IIS 70/E processor, was developed at the Human Factors Laboratory at VPI&SU for softcopy display of both the large and small digital image formats. It is currently in use for soft-copy psychophysical studies paralleling the hardcopy experiments to be described in a subsequent report.

By the end of summer, 1979, a dozen interpretive scenarios had been worked out at Langley AFB. Ten were selected for the psychophysical studies; the others were set aside for purposes of illustration and demonstration, as in this report (see Appendix B). The original 22.9 x 22.9 cm negatives were then transported to Precision Photo Laboratories, Dayton, Ohio, where two high-quality positive transparencies of each were prepared by contact printing. During the printing, each image was gray scale stretched to produce approximately the same maximum dynamic range across all scenes. These transparencies became our "ground truth" data. Because the blurring was to be accomplished by analog means (scanning with large Gaussian apertures at the time of digitization), only positive transparencies could be used without incurring prohibitive computation costs. The positives were ready at the end of September 1979; microdensitometric scanning of the 10 scenes at each of 5 levels of blur could begin. Each of the 50 $(4096)^2$ scans would consume 3 hours. An additional 3 hours would be required to generate each of the 250 (5 noise levels) first-generation positive transparencies on Kodak Technical Pan 2415, to be hand-processed in HC 110-D. Five second-generation positives of each of the 250 transparencies would then be prepared on Kodak Duplicating film, SO-015, by hand processing in Dektol. Hardcopy psychophysical studies were scheduled to begin in mid-July, 1980, and had to be finished

in September. We needed approximately 1000 hours of faultless performance from the Eclipse/PDS microdensitometer between October 1979 and July 1980. It was not to be. The digital interface (of local design and construction) between the microdensitometer and the computer proved unreliable. We had completed only 28 of the 50 required scans and none of the 250 hardcopy displays when we had to abandon it in May to embark on a "crash" program of hardcopy preparation.

FINAL PREPARATION OF DIGITAL DATABASE AND HARDCOPY DISPLAY

Mr. Ray Schmidt of the Image Processing Institute (University of Southern California) generously offered to take on the task of generating the 250 originals from digital tapes supplied by us. His Dicomed D-47, DEC 11/40 installation was already prepared to routinely write 4096 x 4096 pixel images to Kodak 2415 10.16 x 12.7 cm sheet film in 86 mm format, and he had extensive experience in hand-processing this film in Kodak D-19 developer. Though the resolution of the Dicomed is such as to provide no more than 3000 x 3000 independent pixels, our time constraints were such as to encourage acceptance of this limitation. A second major problem attendant to our equipment failure was solved by Mr. H. D. Fisher of the UA's Health Sciences Center. The analog blurring operation via the microdensitometer was now impossible. Mr. Fisher offered to do the blurring digitally by overlapping 9 x 9 $(512)^2$ fast

Fourier transforms, each done "in place" in the large memory of his VAX 11/780. Each of the 10 $(4096)^2$ original microdensitometer scans of the Precision Photo positives would be read to disk, Fourier transformed, and multiplied by four appropriate Gaussian filter functions, thereby creating the spectral versions of the blurred images. These would be inverse transformed to yield, after discarding overlap, the required images. With the very efficient software written by Messrs. Fisher and Kevin McNeill, each scene could be so processed in four hours by the VAX. The blurred image files were then written to tape in internal format, one 16-bit word per pixel, for subsequent input to programs that affected noise additions (five levels), look-up table transformations, and truncation to 8-bit pixels. Thus were the digital tapes prepared for display at the Image Processing Institute.

The Dicomed-written originals were done in "log complement" mode to yield the positives required by our duplicating process. The selection of "log" mode for Dicomed film writing was consistent with the experience of the Image Processing Institute. The look-up tables were designed in such a way as to reproduce the contrast of the original Precision Photo positives in the case of uncorrupted images (10 in number), allowing the remaining 24 versions of each scene to take on the contrast reductions attendant to both blurring and noise addition. The final

copies fell somewhat short of this design goal because of inconsistencies in the exposure and development of both the 250 originals and the 1250 copies. As will be discussed in a subsequent report, these inconsistencies do not appear to have caused any first-order effects in the results of the psychophysical studies.

SUMMARY MEASURES OF DIGITAL DATABASE AND HARDCOPY DISPLAY

In the following two tables we list the nominal and actual values of blur and SNR (peak signal divided by rms noise) exhibited by the digital data recorded on magnetic tape, on the one hand, and its display on SO-015, on the other. The differences result from undesired blurring and noise addition by the Dicomed film recorder.

TABLE 1

Nominal and Actual Blur Values

	Blur Dimension (FWHM in μm)		
Level	Nominal	Tape	SO 015
0	20	22	40
1	40	43	52
2	80	81	84
3	160	161	162
4	320	320	322

TABLE 2

Nominal and Actual Signal-to-Noise Levels

Level	Noise Dimension (SNR_{peak}) Nominal	Tape	SO 015
0	200	200	75
1	100	100	60
2	50	50	42
3	25	25	24
4	12.5	12.5	12

These values of additive noise do not reflect the contribution of the (signal dependent) grain noise exhibited by the positive Precision Photo transparencies, which represent our "ground-truth" data. This contribution is discussed later in the text.

AVAILABILITY OF DATABASE

The digital database, in the form of binary magnetic tapes with 4096 bytes/record, 1 byte/pixel, and 4096 records/image will be available to other investigators when this program terminates. We will not display it in this or subsequent reports, so that future subjects of psychophysical experiments will have had no prior exposure to it. For the same reason, we do not discuss its content, except in most general terms.

The reader may gain an impression of the range of blur and noise covered in the database by referring to Appendix B, where we show degraded versions of an aerial photograph of the US Army Tank and Automotive Command (TACOM), Warren, Michigan.

III. SELECTION OF QUALITY DIMENSIONS OF DATABASE

As noted in the preceding overview, a relevant range of quality parameters was established in several iterations, each involving the preparation of a small set of digitally degraded images, followed by presentation to photointerpreters (PIs) in order to determine the maximum, minimum, and intermediate values of resolution, noise, and contrast. It was our intention at the outset of the program to consider six levels of blur, three levels of noise, and three levels of contrast. Each of these quality parameters independently affects "signal" as perceived in the image. Feedback from PIs suggested that two dimensions of quality reflecting resolution and signal-to-noise ratio would be adequate and realistic. Consequently, image contrast was rejected as an independent dimension, since PIs typically work with transparencies or electronic displays which are optimally contrast-stretched for viewing. A final decision was made to adopt five levels of blur and five levels of noise.

BLUR

PIs indicated that an image quality range of 4 to 8 (or 9) on the 0-9 NATO rating scale is typical of their working environment. In terms of ground resolved distance (GRD), this is a spread of approximately 1.2-1.5 m to 5-15 cm, respectively (see Appendix A). Estimating our ground truth GRD in the Precision Photo positive transparencies to be in the region of 5-8 cm, we adopted five degrees of blur, giving GRD values of approximately 7 cm, 15 cm, 30 cm, 0.6 m, and 1.2 m. The factor of two between blur levels agrees with the NATO and other rating scales, which correlate with logarithmic GRD increments.

NOISE

Consultation with PIs established a maximum rms level of Gaussian additive noise corresponding to a lower limit to our signal-to-noise ratio dimension of 12.5, where signal-to-noise is defined as:

$$\text{SNR} = (\text{peak signal})/(\text{rms noise}). \qquad (1)$$

The selection of intermediate levels in the noise dimension was based on the desire to create subjectively equal increments in noise. It is consistent with Weber's law of psychophysical theory that subjectively equal steps in random grain noise should occur at logarithmic intervals. Zwick and Brothers (1977) report that just-noticeable

differences in rms granularity occur for intervals of 6, 16, or 30%, depending on whether the scene is uniform, "average," or "complex", respectively. Tests involving the addition of Gaussian, uncorrelated noise at different increments in rms level, σ_n, indicated that a factor of two is suitable for coverage of the noise dimension; accordingly, five values of SNR were selected: ground truth (= 200), 100, 50, 25, and 12.5.

CONTRAST

The positive transparencies produced from the original ERIM negatives by Precision Photo Laboratories are of high quality in terms of their tone rendition. They had been prepared in such a way as to satisfy the familiar PI criterion: "Stretch the contrast as far as you can without losing anything." We experimented with several digital algorithms, particularly histogram equalization, as potential candidates for a universal, scene-independent preprocessor. None was found that did not noticeably suppress important details in one or more scenes. We accordingly decided to use the inherent contrast of the Precision Photo transparencies as the design goal of our displays. The undegraded digital images would thus be displayed to match the "ground truth" data in the contrast dimension. The degraded images would then manifest the contrast reductions inherent to the operations of blurring

and adding noise. Scene-dependent contrast stretching, on the other hand, would be regarded as a form of digital processing, to be studied in another phase of the program.

IV. GENERATING THE DIGITAL DATABASE FROM ORIGINAL POSITIVE TRANSPARENCIES

FORMAT OF THE DIGITAL DATABASE

The area scanned from the Precision Photo transparencies for each scene was 82 x 82 mm, this being approximately the size necessary to be representative of the scene content found in tactical photo interpretation. The sampling aperture and interval for digitization was 20 μm, yielding a "ground truth" resolution on the order of 7.6 cm. Each original scene thus provided a matrix of 4096 x 4096 pixels.

Each pixel was ultimately scaled down to 8 bits or 256 intensity levels after the digitization and computer data processing described later. This number of quantization levels, besides being adequate for psychophysical studies, is the standard in most digital image processing hardware, for example, the IIS 70/E at the Digital Image Analysis Laboratory.

A stepwedge was combined with each image at the final stage of blurring and noise-addition for the purpose of photographic calibration in hardcopy production. The stepwedge replaces the last 128 lines of each scene, corresponding to a strip of 2.5 mm width at the edge of the hardcopy format; this strip is divided into 16 blocks having input intensity levels 0, 17, 34, 51, ..., 255.

The block diagram of Figure 2 outlines the steps of the database production, the elements of which are discussed below.

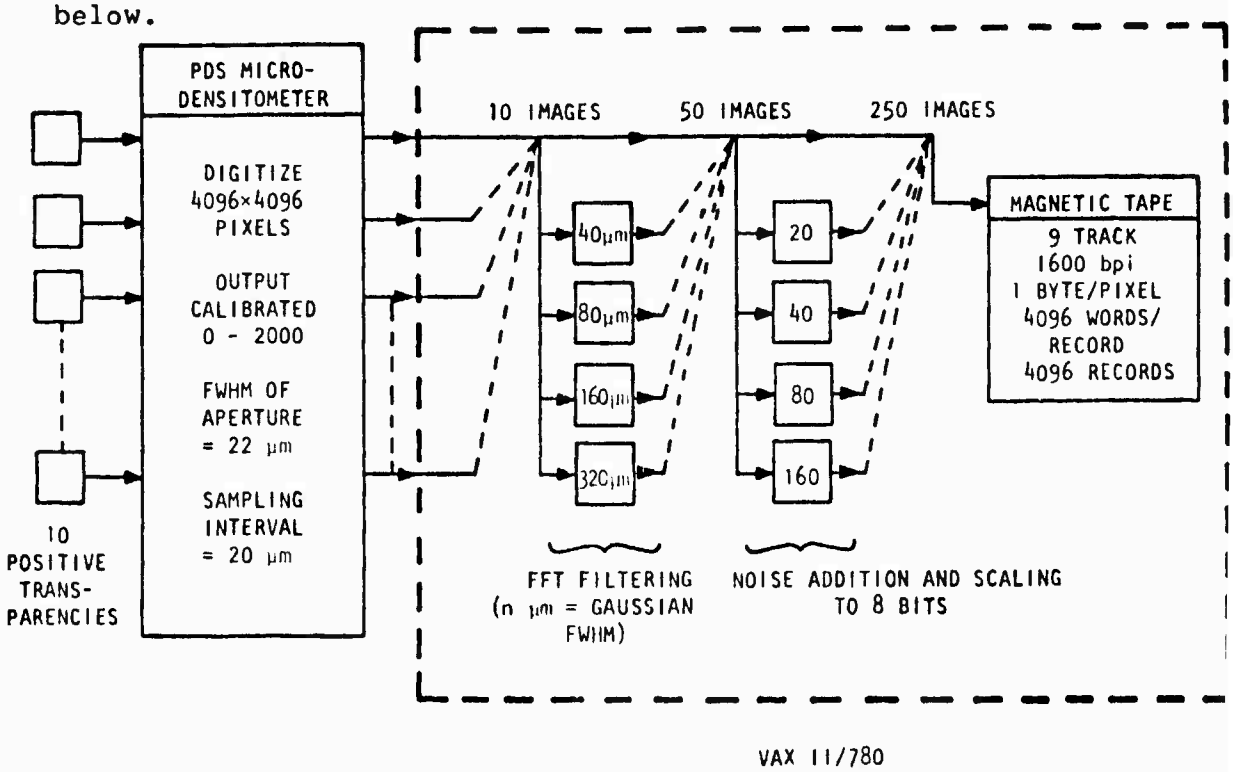

Figure 2: Digital database production

IMAGE IDENTIFICATION CODE, ORDER-OF-BATTLE

A four-digit code identifies each degraded image as follows:

1st Digit:	Photo	0,1,4,5,6,8,9
2nd Digit:	Area within photo	1 or 2
3rd Digit:	Blur level	0 - 4, increasing in blur
4th Digit:	Noise level	0 - 4, increasing in noise

Two non-overlapping areas were selected from each of three Precision Photo transparencies identified as photos 1, 4, and 5. The order of battle for each photo is:

Air: 0, 1, 6

Sea: 4, 5

Land: 8, 9

Throughout this report we often refer to scene 41, say, as a convenient abbreviation of photo 4, area 1.

SCAN CHARACTERISTICS OF THE PERKIN-ELMER PDS MICRODENSITOMETER.

The PDS is capable of generating 12 bits/pixel, i.e., 4096 gray levels. An 11-bit dynamic range, yielding values from 0 to 2000 was convenient for our digitization. The PDS was operated in the transmission mode (number proportional to transmission), with the highest transmission region or highlight within the scene calibrated to N = 2000. Figure 3 shows characteristic curves obtained by scanning a Kodak density wedge with different settings for the minimum density. The gain of the characteristics is essentially unchanged as the highlight calibration varies; it is described by:

$$D = [(D_{min} - D_{max})/\log N_{max}] \log_{10} N + D_{max} . \qquad (2)$$

The above expression is valid over a range of log N of 2.3 (as specified by Perkin-Elmer). Appendix C describes in more detail our use of the microdensitometer and explains the nonlinearities in Figure 3.

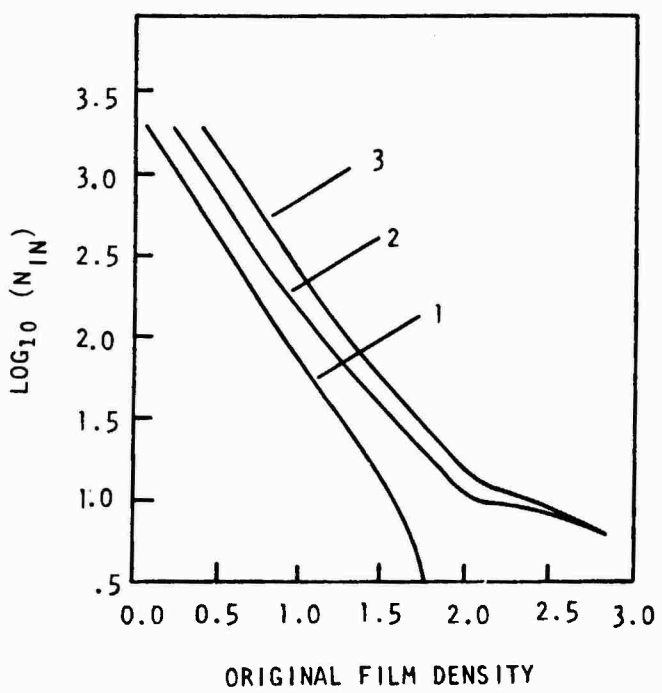

Figure 3: PDS microdensitometer scan characteristic

Ground truth images of 4096 x 4096 pixels were scanned at 20 μm pixel intervals using a square area of dimension 8.19 cm on the Precision Photo original transparencies. The resolution of this scanning aperture is shown in the MTF calibration curve of Figure 4, obtained by scanning bar patterns of known width. Note that the minimum of this approximate sin(x)/x distribution occurs at a spatial frequency of 45 cycles mm^{-1}. This measurement reflects the combined effects of the size of the physical aperture and

the image degradation associated with the optics of the microdensitometer.

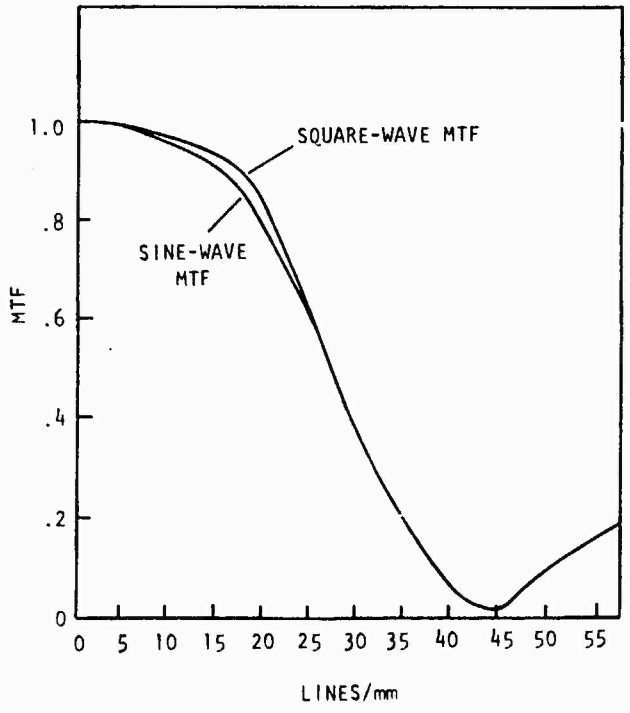

Figure 4: PDS MTF (20 μm aperture)

GRAIN NOISE IN PRECISION PHOTO TRANSPARENCIES

The 10 original scenes were scanned from positive transparencies made by contact-printing 7 ERIM negative transparencies, the film type being either PLUS-X or TRI-X, as shown in Table 3.

Film grain noise in the positives varies according to:

1. The granularity of the negative emulsion (TRI-X is rated 1.65 times as grainy as PLUS-X), and
2. The degree to which the negatives (of varying contrasts and mean density) were contrast-stretched during printing to achieve positives of equal contrast.

TABLE 3

Film Type for Each Image

ERIM Negative Film	Photo #, Area #
PLUS-X	01
	11
	12
	61
TRI-X	41
	42
	51
	52
	81
	91

The classical model of film-grain noise predicts a square-root law between the rms density, σ_D, and the mean density, D

thus:

$$\sigma_D = k(D)^{1/2}. \qquad (3)$$

The constant k is the value of granularity at unit density. The resulting noise in the corresponding digital value, N, is derived using:

$$\log_{10} N = \gamma D_{max} - \gamma D \tag{4}$$

$$\sigma_N = [dN/dD]\sigma_D. \tag{5}$$

Thus

$$|\sigma_N| = [\gamma Nk/0.4343][(D_{max} - (\log_{10} N)/\gamma))]^{1/2}, \tag{6}$$

or,

$$N/|\sigma_N| = [0.4343/\gamma k][(D_{max} - (\log_{10} N/\gamma)]^{-1/2}, \tag{7}$$

where:

$0 \leq N \leq 255$

γ = gamma of PDS characteristic.

Figure 5 gives curves of "signal-to-noise" (N/σ_N) versus N for each photograph. These were obtained by varying k in order to test the fit of the expression for $N/|\sigma_N|$ to three or four measurements of σ_N taken at intervals in N between 0 and 255 in local image regions of apparently uniform intensity (i.e., no visible structure apart from grain noise.)

In addition to the intentional noise of four levels (σ_N = 20, 40, 80, 160), we therefore have a source of signal-dependent noise to consider in the digital database. The fact that this noise is introduced before blurring means that it is halved with each increasing level of blur. A third, additive source of noise in the hardcopy database is discussed in Appendix E.

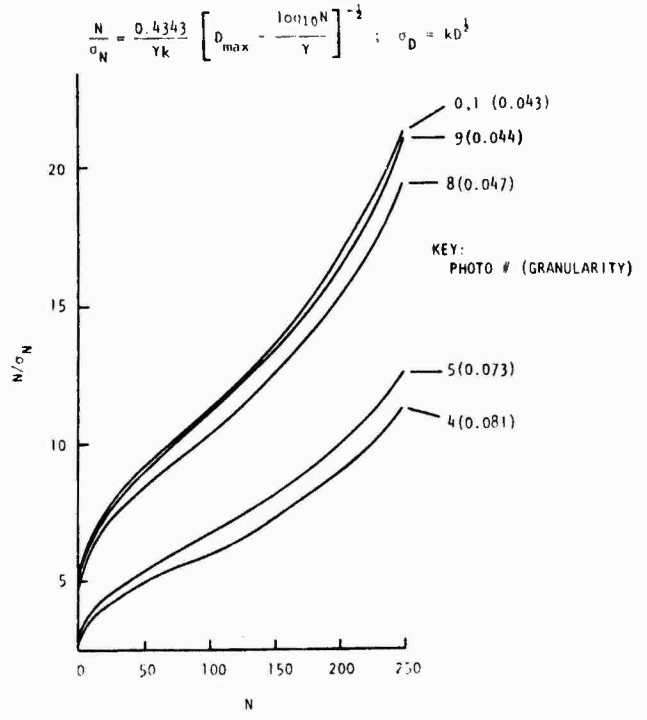

Figure 5: Grain noise in Precision Photo transparencies, σ_N = rms noise

COMPUTER PRODUCTION OF BLURRED, NOISY IMAGES FROM GROUNDTRUTH BLUR

Blur

It was our original intention to accomplish blurring by scanning the Precision Photo transparencies using Gaussian apertures manufactured by exposing the necessary transmission distributions on film. The four blur-widths corresponding to our range of GRD would be: R_h = 40, 80, 160, 320 μm, where R_h is the full-width at half maximum (FWHM). The usual measure of Gaussian width σ_b (standard deviation) is related to R_h by $\sigma_b = 0.425\ R_h$. Because the images are sampled on the PDS at 20 μm intervals, it is useful to specify values of σ_b as 0.849, 1.699, 3.398, and

6.795, measured in units of inter-pixel distance. In reality, analog blurring proved impossible due to equipment failure causing us to adopt a digital method.

The technique of block-mode filtering by Fast Fourier Transforms was implemented by H. D. Fisher of the University of Arizona's Health Sciences Center on the VAX 11/780 computer. This method, shown in schematic form in Figure 6, is equivalent to convolving the original digitized data with four 64 x 64 Gaussian point spread functions of widths b given above. In block-mode filtering, each of 81 (i.e., 9 x 9) partially overlapping blocks of 512 x 512 pixels was Fourier transformed in the VAX memory and multiplied by the appropriate filter (the Fourier transform of the Gaussian point spread function in our case). After inverse transformation, the 32-pixel wide border is discarded and output blocks of 448 x 448 pixels are set out contiguously as in Figure 6. The exception to this occurs at the edges of the 4096 x 4096 matrix, where only the inside borders of the 512 x 512 blocks are discarded, leaving output blocks of 480 x 480 pixels in each corner and 480 x 448 pixels along the edges. The expected wraparound effect in a 32-pixel wide strip at the outermost border is not evident in our images. The computer processing time expended in generating the 4 blurred versions of each of the 10 4096 x 4096 scenes was 4 hours.

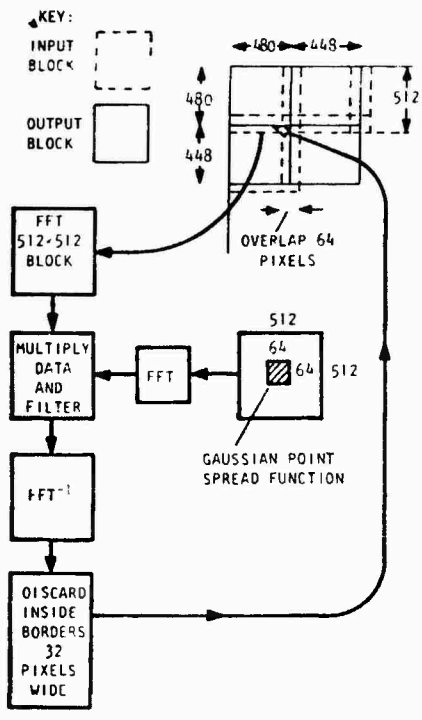

Figure 6: Blurring by block-mode filtering

We have determined by experiment that the resulting effective GRD is related to σ_b by

$$GRD = 2.5\ \sigma_b \tag{8}$$

This relation is valid even for truncated Gaussian point spread functions, provided that the extent of the function is at least 3 σ_b. For the case of airport #1, Scene 01, for example, we therefore have GRDs of ground truth, 18, 35, 71, and 142 cm (based on a photographic scale factor of 4400:1 for this scene).

Noise.

The next stage in image [illegible] generation of a single digital file of 4096 x 4096 pixels of random Gaussian noise, which was then to be weighted and added to each blurred scene. During initial tests with 512 x 512 image arrays, we created pairs of uniformly distributed random numbers (rv_1 and rv_2) using the IBM FORTRAN routine RANDU for subsequent computation of Gaussian random numbers via the following algorithm:

$$g = \sigma\,(-2\,\log_e\,rv_1)^{1/2}\,\cos\,(2\,\Pi\,rv_2). \qquad (9)$$

It was found, however, that this algorithm periodically generates highly correlated structure over an area of 4096 x 4096 pixels. (Forsythe, Malcolm, and Moler, 1977, report a similar phenomenon, and have written a superior algorithm URAND.) We subsequently generated the large uncorrelated noise file more economically by scanning a uniformly exposed photographic emulsion, developed to a density of unity, using a small (10 μm) aperture in the PDS microdensitometer. After subtracting the mean value, the noise statistics remain approximately Gaussian (see Figure 7), where the standard deviation is approximately 40 intensity units. Hence, with the original database still within the range 0 to 2000, noise weighting factors of 0.5, 1, 2, and 4, applied to this noise file, provided the desired values of additive noise.

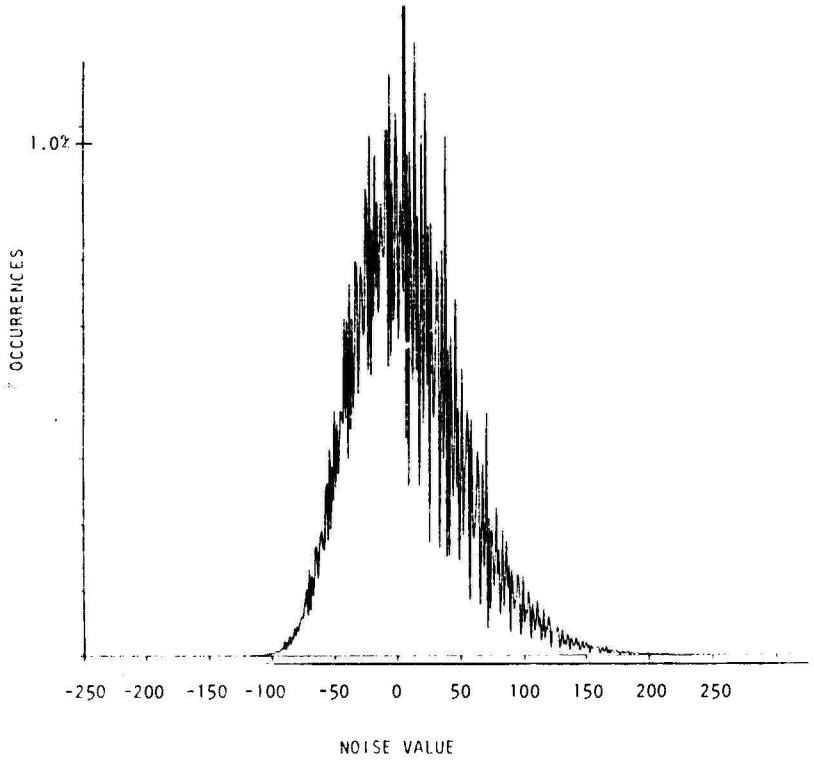

Figure 7: Noise histogram

SUMMARY MEASUREMENTS OF QUALITY AND STATISTICS OF DIGITAL DATABASE

As previously mentioned, the digital database is in 8-bit format on 9-track tape with 4096 bytes (pixels)/record and 4096 records/image file.

Blur

Table 4 compares actual and nominal values for the effective FWHM of the Gaussian point spread functions for each level of blur. The small deviations from nominal are caused by the combined effects of the PDS scanning aperture and the imaging optics.

TABLE 4

Nominal and Actual FWHM (μm)

Level	Nominal Blur	Digital Database on Magnetic Tape
0	20	22
1	40	43
2	80	81
3	160	160
4	320	320

Noise

The level of noise introduced during scanning by the PDS microdensitometer is negligible. The four nominal values for rms noise were obtained: σ_n = 2.5, 5, 10, 20 (8-bit scale).

Histogram-Related Statistics

We used a 512 x 512 subsampling of each of the 4096 x 4096 images to derive global histogram statistics. Figure 8 and Tables 5 and 6 show maxima, minima, and means for blur levels 0, 2, and 4. They also list the values of a parameter called %-dynamic range, this being a measure of the limiting gray levels above and below which reside x% of the total number of pixels. For example, 90%-dynamic range at 194 and 14 means that 5% of all pixels have gray levels less than 14 and 5% have gray levels greater than 194.

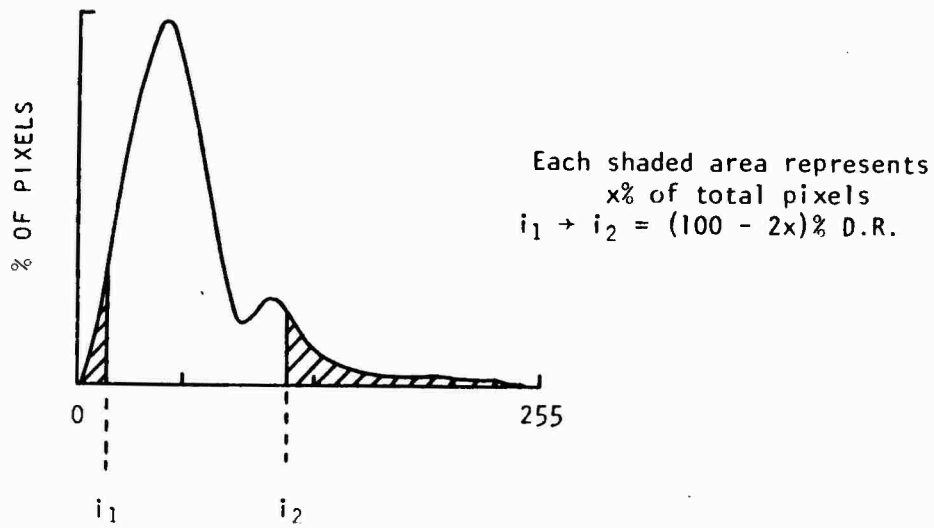

Figure 8: Illustration of % D.R. (dynamic range)

Image histograms for the 10 scenes at blur level 0 are shown in Figure 9, and histograms for scenes 01, 41, and 91 at blur levels 2 and 4 are given in Figure 10 (a-f). Several histograms are noticeably bi- or tri-modal; all are biased toward the zero signal or high density end of the scale. The port scenes from photo 4 (scenes 41 and 42) exhibit somewhat broader gray-level distributions, particularly scene 41. Figure 11 illustrates the potential utility of the %-dynamic range values as measures of the image "contrast" or "peak-to-peak" signal. For example, scenes 81, 91, and 12 possess almost identical true peak-to-peak values, yet the spread in their 90% dynamic range figures is large. The higher proportion of highlight densities for scene 12 is also evident in the shape of the

TABLE 5

First Order Statistics for 10 Scenes, Blur 0, Noise 0.

Image #	Max;Min	Mean	98%	D.R.	90%	D.R.	80%	D.R.
0100	233 0	38	158	2	103	2	89	2
1100	227 0	23	122	2	91	3	67	4
4100	255 0	51	140	7	109	9	96	12
5100	207 0	17	131	2	82	3	45	3
6100	255 0	70	255	1	235	2	176	14
8100	244 0	11	99	2	37	3	21	3
9100	240 0	28	173	2	92	3	72	4
1200	239 0	30	179	2	109	3	88	4
4200	210 0	28	93	5	72	6	61	7
5200	203 0	11	83	2	45	2	31	3

TABLE 6

Histogram Statistics for Representative Scenes, Blurs 2 (top) and 4 (bottom), Noise 0.

Image #	Max;	Min	Mean	98%	D.R.	90%	D.R.	80%	D.R.
0100	228	0	28	156	2	101	2	88	2
4120	255	4	51	125	7	102	9	92	12
9120	233	1	28	170	3	90	3	71	4
0140	244	0	38	150	2	99	2	86	2
4140	255	4	51	119	8	100	10	91	13
9140	230	1	28	162	3	87	3	69	5

histogram. These histograms illustrate the familiar difficulties that arise when one attempts to find a universal, psychophysically meaningful definition of "signal" in an optical image.

We recall from Figure 2 that there is no renormalization after the blurring process (FFT-filtering); hence, we would expect a post-convolution histogram to be slightly reduced in dynamic range, and its shape altered somewhat, particularly in the highlight range where structure tends to be fine and therefore most susceptible to blurring. Figure 12 illustrates the effect of blur (levels 2 and 4) on the dynamic ranges for scenes 01, 41, and 91. There appears to be no major scene-dependent effect caused by blurring of

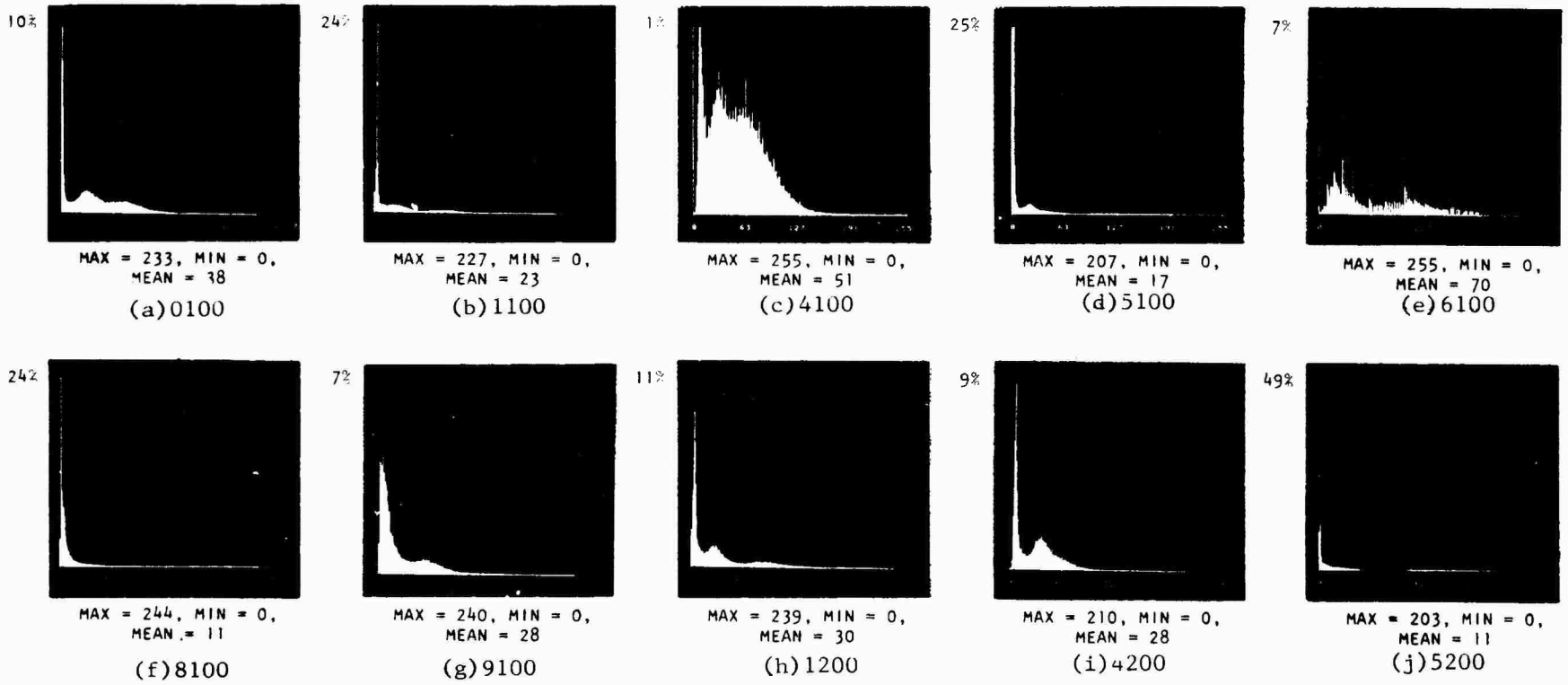

Figure 9: Digital database histograms (Blur 0, Noise 0). % value is maximum percentage of occurrences of most frequent intensity.

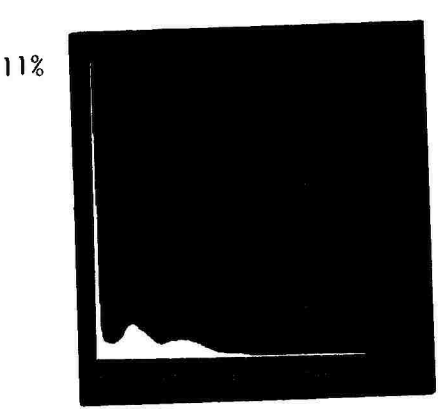

MAX = 228, MIN = 0, MEAN = 38

(a) 0120

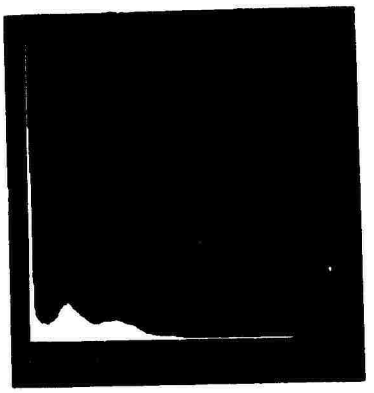

MAX = 224, MIN = 0, MEAN = 38

(b) 0140

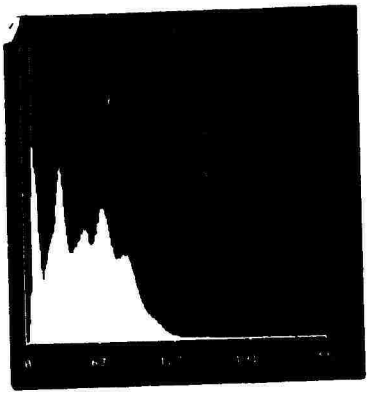

MAX = 255, MIN = 4, MEAN = 51

(c) 4120

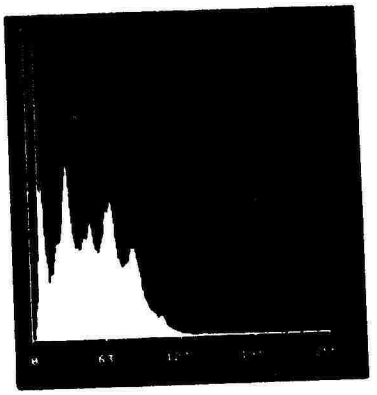

MAX = 255, MIN = 4, MEAN = 51

(d) 4140

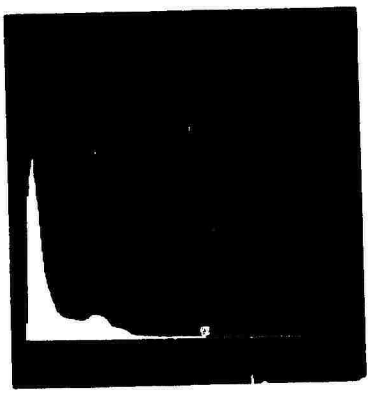

MAX = 233, MIN = 1, MEAN = 28

(e) 9120

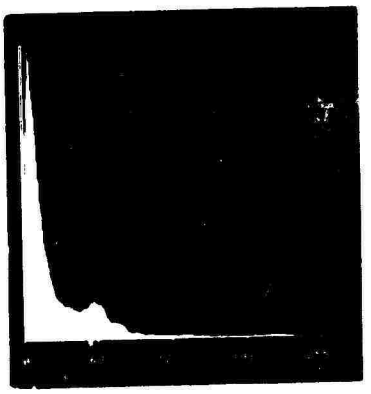

MAX = 230, MIN = 1, MEAN = 28

(f) 9140

Figure 10: Representative digital database histograms (Blurs 2, 4: Noise 0)

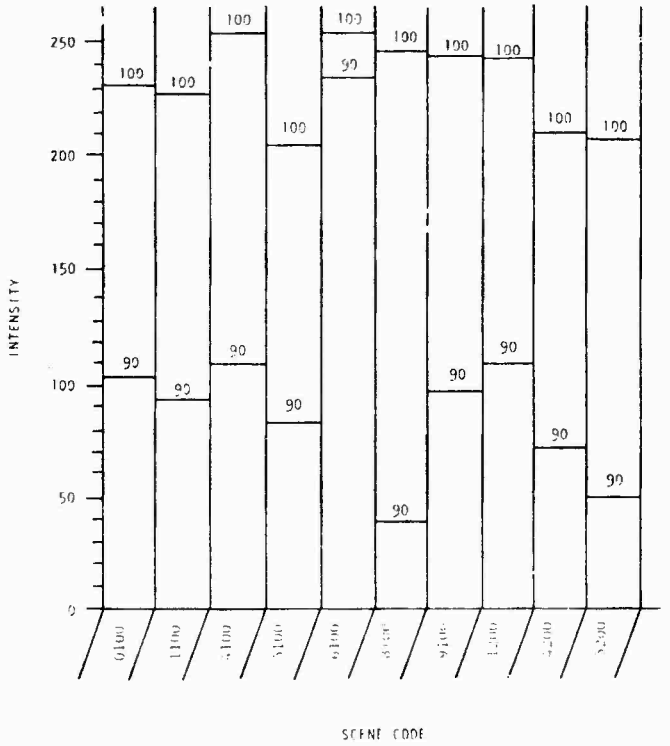

Figure 11: Peak-to-peak and 90% dynamic range, Blur 0

highlights, since the spread of dynamic range with blur for 100, 98, and 90% levels is approximately constant within scenes. All three measures of dynamic range remain roughly constant throughout the blur dimension. We do not reproduce here the histogram for blurs 2 and 4 for every scene because the relationship among their dynamic range values with blur is essentially equivalent to those shown.

In understanding the shape of a histogram after the addition of noise there are two factors to consider. First, the histogram of the combined image (image file plus noise file) is akin to the convolution of the histograms of the separate components. The simplest example is the addition of zero-mean Gaussian noise to an image of uniform intensity, k; the composite histogram is obtained by

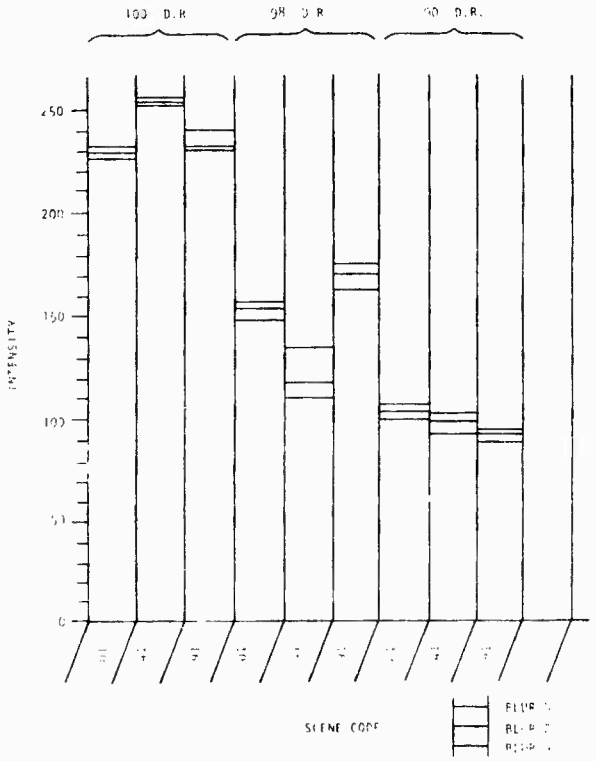

Figure 12: Effect of blur on dynamic range, zero noise

convolving a Gaussian function with a delta function, the result being a Gaussian histogram shifted to a mean level k. Notice also that the inherent smoothing associated with convolution causes considerable reduction of the absolute value of the peak in the uniform histogram.

The second factor results from the fact that noise addition was performed by combining the 11-bit (positive) signal data with 11-bit (positive and negative) noise data. The resulting data were lmited in dynamic range by setting negative values equal to 0 and values exceeding 4095 (12 bits) equal to 4095. This "scaling" accentuates the histogram at the end of the gray level range towards which the original histogram was biased. Both factors are apparent in the histogram of scene 91 at blur level 0 and

noise level 4, shown in Figure 13. When scaled to 8 bits, a total of 24% of the image pixels are at level 0 due to the addition of noise of standard deviation 20 (8-bit scale) to an image whose mean level is 28.

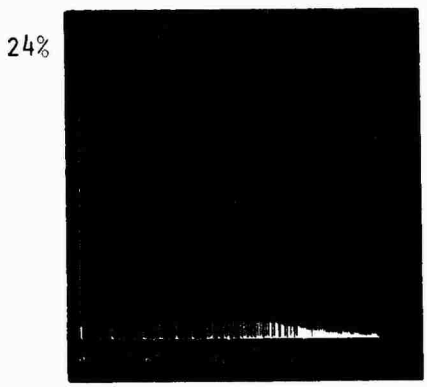

Figure 13: Digital database histogram (Noise 4)

V. GENERATING THE HARDCOPY DATABASE

FORMAT OF HARDCOPY

The task of generating hardcopy was transferred from the UA PDS microdensitometer to the Dicomed D-47 at the USC Image Processing Institute. Our specifications called for hardcopy display of positive transparencies written on Kodak Technical Pan 2415 at the same scale as the original Precision Photo originals. Playback should therefore have been at pixel spacing of 20 μm, equal to PDS digitization. In reality, the Dicomed operates at 21 μm pixel spacing, yielding slightly larger hardcopy, having a final reproduction scale of 86 mm:82 mm or 1.05:1. A requirement for five copies of each 2415 transparency for PI experiments necessitated positive contact printing on Kodak SO-015 duplicating film. The format of the hardcopy films is shown in Figure 14.

PLAYBACK CHARACTERISTICS OF THE DICOMED

The Dicomed D-47 image writer, operating in its "high resolution" mode, generates a matrix of pixels spaced at intervals of 21 μm, each pixel having one of 256 gray levels corresponding to an ultimate film density, in Kodak Technical Pan 2415, determined by various electronic

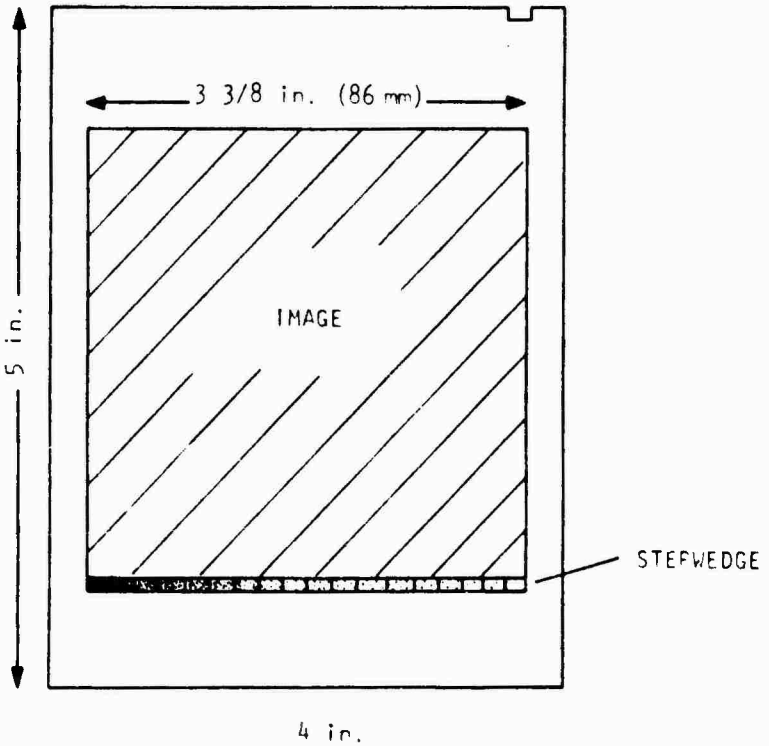

Figure 14: Hardcopy format, Kodak 2415

calibrations of the instrument as well as the final darkroom processing in D-19 developer. Appendix D gives the manufacturer's specifications for this instrument.

Resolution, MTF.

Dicomed resolution is specified by the manufacturer to be 3000 lines over the plotting matrix, equivalent to 18 lines (pairs)/mm. Figure 15 shows two MTF curves derived by scanning bar patterns recorded by the Dicomed onto 2415 in orthogonal directions; the bars have various widths and originate from the Dicomed operating in "high resolution" mode. The modulation caused by the 10 μm aperture employed in this microdensitometer measurement has been removed, along with the transformation from square wave to sine wave

MTF. Clearly, the Dicomed resolution falls short of our intended goal of reproducing, at high contrast, frequencies up to 50 lines/mm.

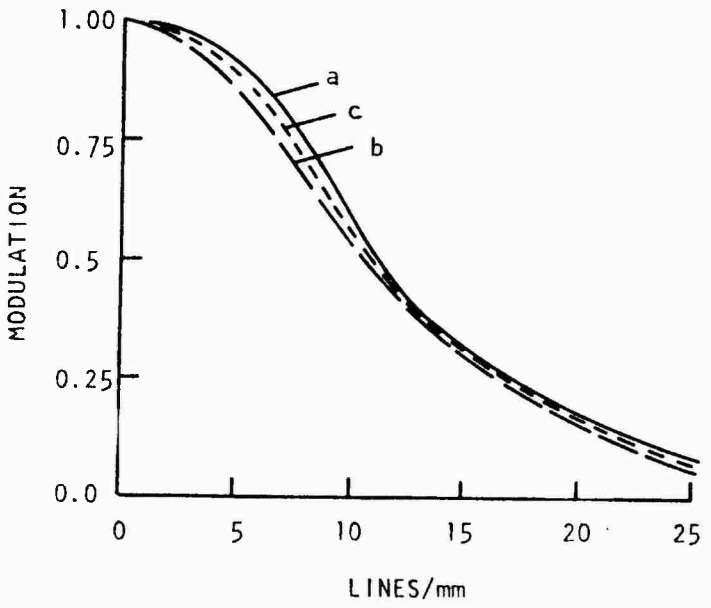

Figure 15: Dicomed MTF: (a) orthogonal to scan direction, on, (c) average of a and b. (b) parallel to scan direction, (c) average of (a) and (b)

Noise

Fluctuations in density are evident in the step wedges written by the Dicomed on the 2415 transparencies, as well as the SO-015 duplicates. The fluctuations are correlated over a distance of 40 μm (where the correlation coefficient equals 0.1), which is the approximate diameter of a pixel written by the Dicomed. We conclude that this Dicomed noise arises from fluctuations in the charge delivered to the

phosphor when the Dicomed beam is unblanked. It is probably associated with fluctuations in accumulated space charge during periods when the beam is blanked. This noise represents an independent, uniform, additive, uncorrelated contribution to the noise added digitally. Its numerical equivalent, in units of the digital database, is given by σ_N(Dicomed) = 3.33. This number was determined as described in Appendix E.

A second, less serious noise was the apparent outcome of geometric inaccuracy[1], manifest as dark raster lines when viewed under high magnification (60X), appearing to be spaced at periodically varying intervals of, typically, 100 μm. We feel that this form of "noise" is clearly discernible as being a display defect rather than being genuine scene structure. Another manifestation of geometric error was seen intermittently in the form of single skewed lines; one such example exists within our hardcopy database in scene 5200, located 2 mm from the stepwedge. Playbacks whose information content was seriously affected by such anomalies were repeated. The Dicomed also introduces three faint lines perpendicular to the scan direction, their spacing being such as to divide the 4096 x 4096 plotting matrix into four equal sections. We presume this to be an artifact of the D/A converter that controls the voltage

---

(1) Dicomed geometric accuracy is specified in: Operational and Programming Manual, Image Recorders, Models D46 and D47, Dicomed Corporation, 9700 Newton Avenue, South, Minneapolis, MN 55431.

supplied to the deflection yokes of the CRT.

Tone Reproduction

Hardcopy on Kodak 2415 was written with the Dicomed set in its "log complement" mode, i.e., output density linear with input number. The "positive" numerical data input to the Dicomed therefore resulted in a positive transparency. Tests of Dicomed playback revealed occasional anomalous behavior, manifest as one or more highly non-linear regions in a normally near-linear curve. Figure 16 compares an example of this behavior with the normal case. We could only speculate as to the source of this disturbing effect; we surmise that it is caused by non-uniform phosphor response across the CRT of the Dicomed. The Dicomed has a "priming mode", designed to obviate phosphor hysteresis; however, evidence of questionable post-priming operation persuaded us to ignore this feature and keep the device switched on throughout the film recording process. Curve C of Figure 16 is typical of calibrations run immediately after priming. Curve B is more representative of our data as recorded on 2415, though some flattening of the characteristic at intermediate and high values, to a lesser extent than that illustrated by curve C, often and unpredictably occurred.

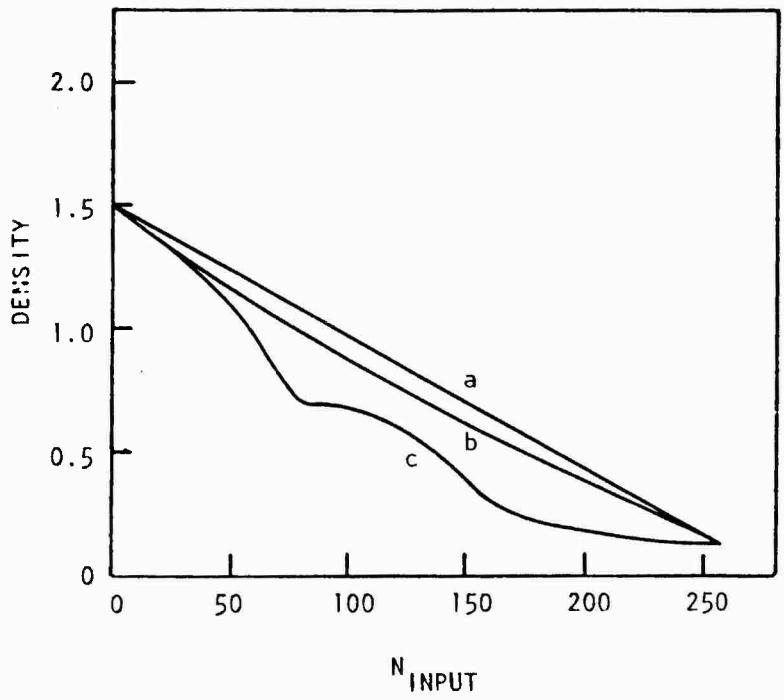

Figure 16: Dicomed tonal transfer: (a) ideal, (b) acceptable, (c) unacceptable

Generating Transfer Curves for Playback

Our previously stated aim for tone reproduction in playback was to maintain the contrast of the original Precision Photo positives. Because we scanned the ground truth database in "transmission-mode", there was a requirement to perform a logarithmic transformation on the digital database prior to hardcopy generation on the Dicomed, whose characteristic is to yield densities approximately linear with input number. Also, an additional compensatory transfer curve or look-up table (LUT) was needed in view of the nonlinearity of the Kodak SO-015 duplicating film.

Design of LUTs was based on a modification relationship between the photometric input to a photographic system and the output of that system, expressed in terms of the final photographic density (Tupper, 1966). In Figure 17, quadrants 1 and 3 are known through instrument and development calibration (quadrant 3 is the composite Dicomed/2415/SO-015 curve), and quadrant 4 is the desired goal of tone reproduction.

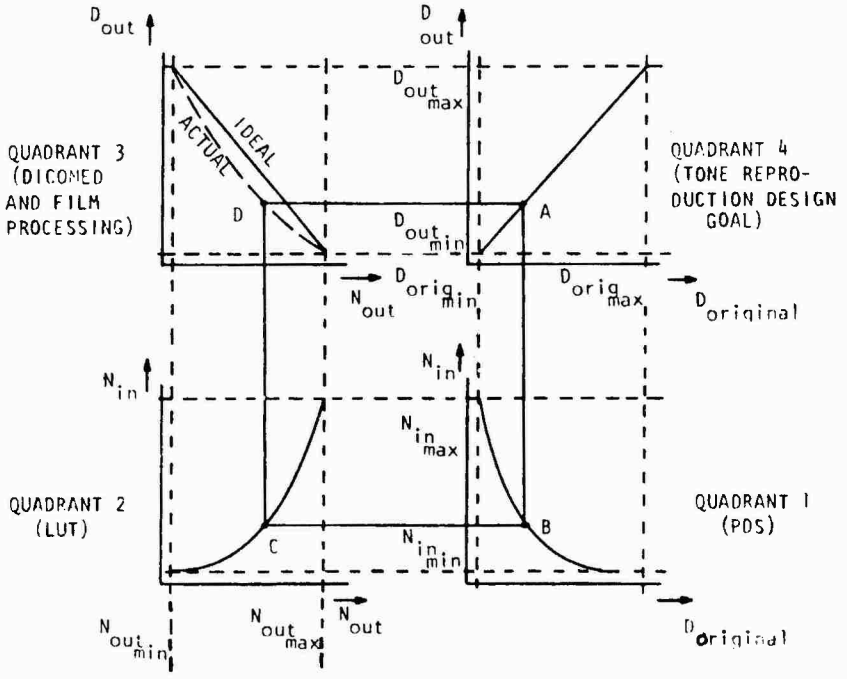

Figure 17: LUT design

It remains to calculate the LUT needed in quadrant 2 to provide a "match" between the digital database and the SO-015 display. A certain output density, corresponding to the original density at point A, is traced vertically downwards to point B, locating the equivalent transmission

value N_{IN} in the digital database. Once again, starting at point A, the input needed to produce the same value of output density on the playback curve is located by tracing horizontally to point D. It is then a simple matter to link points B and D to give a point C on the LUT. Additional points covering the required range of output density are then employed to define the complete LUT.

The idealized (and unrealizable) case of a linear Dicomed/contact-processing characteristic gives a logarithmic LUT:

$$N_{out} = N_{out_{min}} + (N_{out_{max}} - N_{out_{min}})/(\log N_{in_{max}} - \log N_{in_{min}}) \cdot (\log N_{in} - \log N_{in_{min}}) \qquad (10)$$

which, assuming:

$$N_{out_{min}} = 0, \quad \log N_{in_{max}} = \log 255,$$

$$N_{out_{max}} = 255, \text{ and } \quad \log_{in_{min}} = 0,$$

gives:

$$N_{out} = (255/\log 255) \log N_{in}. \qquad (11)$$

In reality, the composite playback curve is somewhat nonlinear, as Figure 17 shows; actual LUTs were therefore less curved than the above equation suggests. Figure 18 illustrates the three LUTs that were used, and identifies

the associated blur levels: (i) 2, (ii) 0, and (iii) 4, 3,1; (i) - (iii) also represent the order of our production schedule. The variability between (i) - (iii) may be attributed to two factors: the fluctuation in Dicomed performance and USC darkroom-processing stability, and our increasing understanding of how the Dicomed photo-processing affected playback quality and how to optimize LUT designs to compensate for observable "anomalies", such as gross non-linearities in the Dicomed curve. In retrospect, the final LUT (iii) represents our best compromise, which, had the time been available, should have been used for blur levels 2 and 0 also. Notice that the dynamic output range is 0 to 243, rather than 0 to 255. This is to compensate for the tendency of the playback curve to "flatten out" between 243 and 255 because of Dicomed nonlinearity.

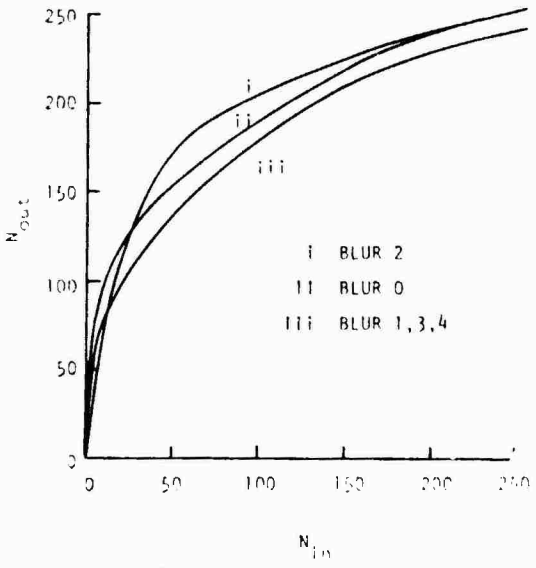

Figure 18: LUT curves

SUMMARY MEASURES OF QUALITY AND STATISTICS OF HARDCOPY DATABASE

Blur

An approximate representation of the composite MTF for each degree of blur, with no noise added, is shown in Figure 19. The five curves are derived by cascading in sequence three MTF curves: the PDS MTF, the effecive MTF of digital blurring, given by exp $\{(-1/2)(2\pi f\sigma)^2\}$, and, finally, the average Dicomed MTF.

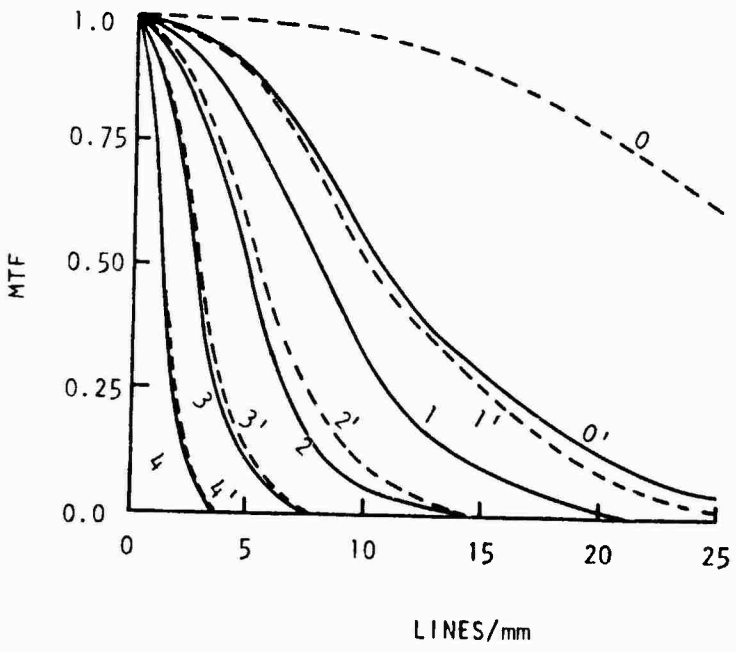

Figure 19: Composite hardcopy MTF at each blur level. Solid lines are ideal (infinite Dicomed resolution)

Table 7 compares nominal and realized hardcopy blur levels.

TABLE 7

Nominal and Actual Hardcopy FWHM Blur (μm)

Level	Nominal	Hardcopy
0	20	40
1	40	52
2	80	84
3	160	162
4	320	322

The disparity is created by the relatively poor performance of the Dicomed (Figure 15), and is clearly most serious at levels 0 and 1. Hardcopy blur level 0 is approximately the same as the nominal value of 40 μm of blur in level 1.

Noise

As noted above, the Dicomed contributed an equivalent uncorrelated additive noise to our digital database of rms value 3.33. Adding this in quadrature with the added noise digitally produced the actual SNR levels (peak signal to rms noise) in the hardcopy indicated in Table 8.

TABLE 8

Nominal and Actual Hardcopy SNRs

Level	Nominal SNR	Hardcopy
0	200	75
1	100	60
2	50	42
3	25	24
4	12.5	12

Histogram-Related Statistics, Tone Reproduction

The hardcopy data shown in Table 9 and the density histograms of Figure 20 (a-j) and Figure 21 (a-g) were simulated on the International Imaging Systems 70/E image computer in the Digital Image Analysis Laboratory at the University of Arizona. Images of 512 x 512 pixels, which were derived by subsampling the digital database at every eighth pixel, were stored in 8-bit refresh memory and hardware LUTs applied in the IIS 70/E pipeline processors in order to simulate the tonal transfer curves and playback curves of our actual hardcopy displays. We have already discussed the tonal transfer curves of Figure 18. We assumed for our simulation of hardcopy that the shape of the playback characteristic remained constant as the maximum densities varied with each scene in the degraded database.

(By "playback characteristic" we mean the composite curve of the Dicomed/2415/SO-015.) Measurements taken from hardcopy production supported the above assumption. The resultant density histograms of Figures 20 and 21 are essentially indistinguishable from those of Figures 9 and 10 with logarithmic LUTs applied. It should be noted that the abscissa scale of 0 - 255 for Figures 9, 10, and 13 represents data values ranging from 0 to 255. In Figures 20 and 21, the 0 - 255 scale is quite arbitrary. It is a linear scale in density, where $0 \equiv D_{max}$ and $255 \equiv D_{min}$. (D_{min} always lies in the range 0.13 - 0.15.)

Figure 22 compares the tone reproduction of every blur level with the ideal that we set out to achieve, each curve being derived by cascading the playback curve, LUT (from Figure 18), and PDS curve. The scale of the ordinate value assumes that we achieved the correct maximum density. Cases where this is not so require appropriate correction (see Appendix D). Reproduction of contrast for blur level 2 is obviously the worse case. A tendency toward "washed-out" highlights and obscured backgrond details is the result. Ironically, some mid-range structure is enhanced, as in deck structure on the vessels of port scene 51. A casual observer would no doubt notice the different contrast of blur level 2 scenes. It remains to be seen whether our PI studies reveal any disparity in performance caused by the three tonal transfer curves. The variation in contrast

among the remaining blur levels is not apparent in our hardcopy, as perhaps Figure 22 indicates.

TABLE 9

Hardcopy Density Histogram Statistics

Image #	Max;	Min	Mean	98%	D.R.	90%	D.R.	80%	D.R.
0100	1.85	.15	0.78	1.60	.17	1.60	.26	1.60	.29
1100	2.2	.15	1.00	1.96	.24	1.71	.33	1.59	.44
4100	2.03	.14	0.56	1.12	.18	1.05	.26	0.95	.29
5100	1.88	.15	1.09	1.67	.20	1.47	.34	1.47	.51
6100	1.85	.14	0.54	1.84	.14	1.65	.14	0.82	.16
8100	1.91	.15	1.06	1.69	.28	1.48	.57	1.48	.72
9100	1.99	.15	0.94	1.79	.17	1.54	.33	1.49	.44
1200	1.84	.15	0.86	1.65	.16	1.45	.25	1.35	.29
4200	1.89	.15	0.77	1.28	.29	1.17	.37	1.07	.42
5200	1.94	.15	1.21	1.73	.32	1.73	.51	1.52	.63
0120	1.9	.15	0.84	1.82	.17	1.80	.22	1.80	.25
4120	1.79	.14	0.55	1.55	.19	1.43	.22	1.25	.25
9120	1.63	.15	0.86	1.53	.16	1.53	.55	1.45	.26
0140	1.85	.15	0.80	1.65	.17	1.65	.26	1.65	.29
4140	1.41	.15	0.62	1.19	.26	1.12	.30	1.02	.34
9140	1.75	.16	0.96	1.65	.18	1.63	.37	1.45	.45

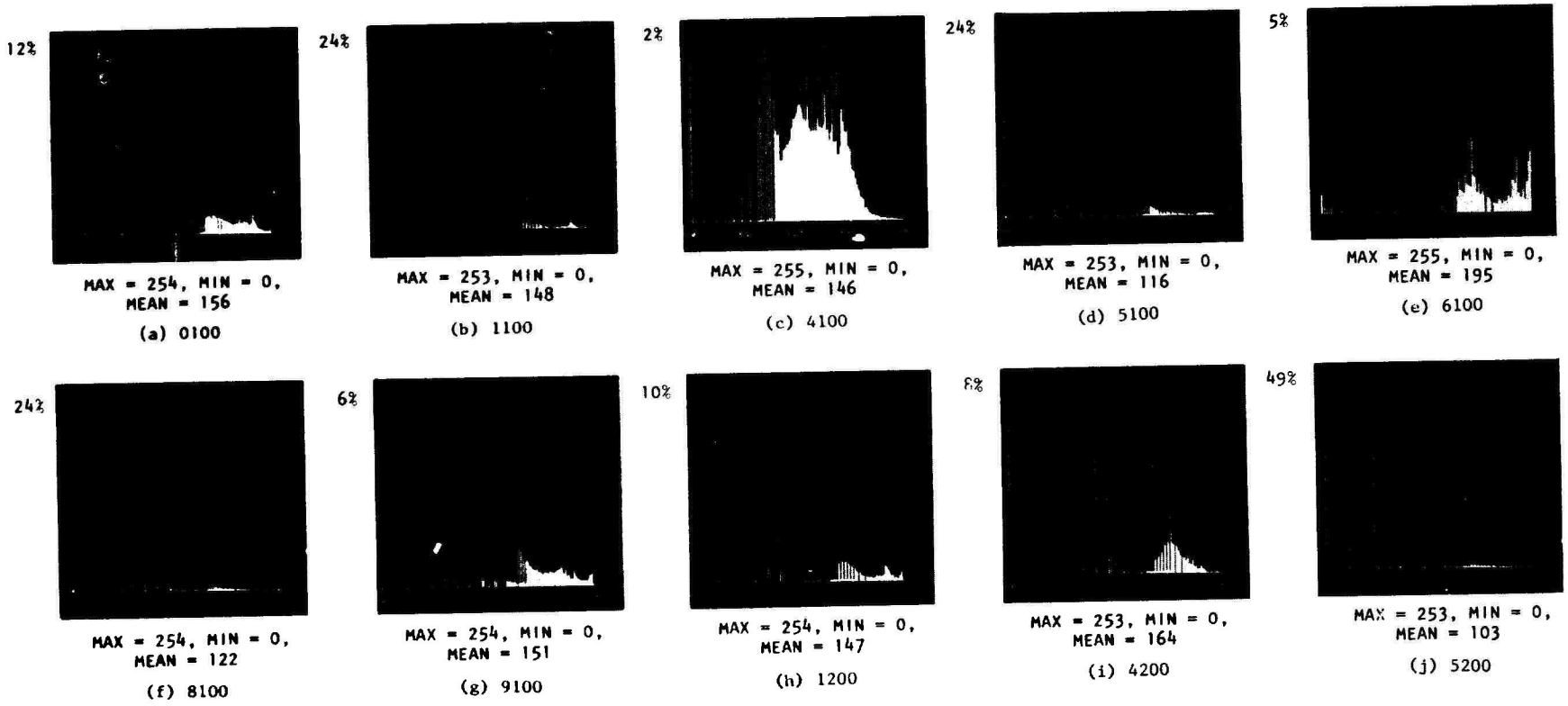

Figure 20: Hardcopy histograms (Blur 0, Noise 0). Abscissa scale. 0 D_{max}, 255 D_{min}. (D_{min} = 0.13 - 0.15.)

Values of D_{max};

(a) 1.85, (b) 2.20, (c) 2.03, (d) 1.88, (e) 1.85, (f) 1.91, (g) 1.99, (h) 1.84, (i) 1.89, and (j) 1.94.

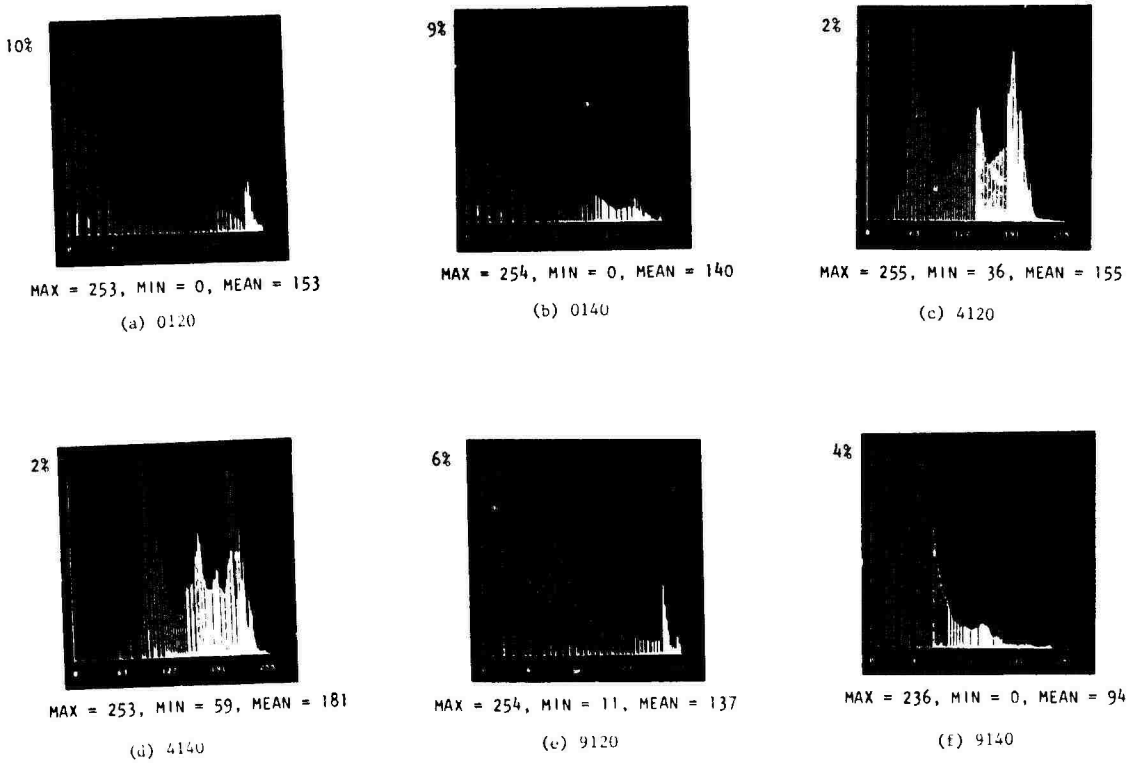

Figure 21: Representative hardcopy histograms (Blurs 2, 4: Noise 0). Abscissa scale: $0 \equiv D_{max}$, $255 \equiv D_{min}$ (D_{min} = 0.13 - 0.15.)

Values of D_{max};

(a) 1.9, (b) 1.85, (c) 2.1, (d) 1.79, (e) 1.7, and (f) 1.83.

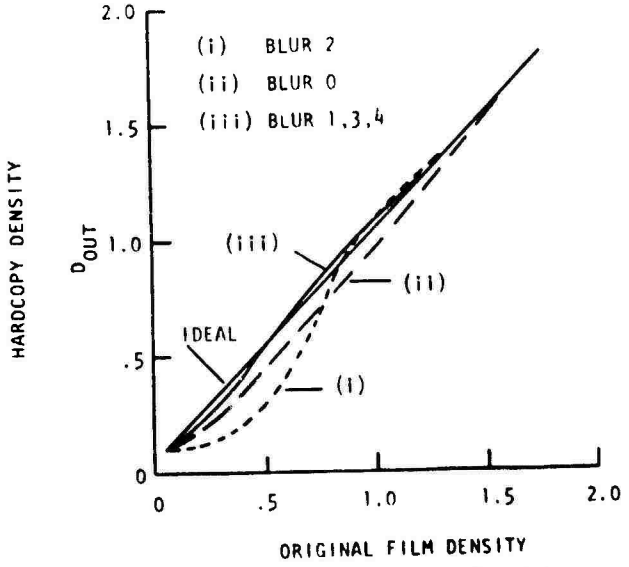

Figure 22: Hardcopy tone reproduction.

Table 10 given the measured maximum density of all 250 scenes from the selected dark regions described in Table 11.

TABLE 10

Hardcopy Maximum Scene Densities

	Noise Level				
	0	1	2	3	4
010	1.58	1.85	1.68	1.27	1.23
011	1.74	1.73	1.55	1.56	1.45
012	1.78	1.32	1.52	1.44	1.26
013	1.71	1.78	1.54	1.63	1.35
014	1.74	1.72	1.65	1.64	1.45
110	1.60	1.70	1.69	1.73	1.57
111	1.60	1.58	1.66	1.56	1.47
112	1.98	2.07	1.98	2.21	1.85
113	1.41	1.48	1.49	1.69	1.69
114	1.60	1.63	1.63	1.77	1.50
410	0.97	1.23	0.89	1.00	1.12
411	1.24	1.30	1.31	1.40	n/a
412	1.59	1.41	1.26	1.55	1.26
413	1.23	1.24	1.28	1.30	1.20
414	1.15	1.18	1.00	1.23	1.10
510	1.82	1.81	1.73	1.60	1.15
511	1.32	1.48	1.46	1.52	1.38
512	2.22	2.04	2.31	2.10	2.09
513	1.62	1.57	1.53	1.44	1.31
514	1.74	1.71	1.59	1.59	1.51
610	0.69	0.74	0.86	0.90	1.10
611	1.44	1.44	1.46	1.53	1.44
612	1.54	1.88	1.51	1.16	1.50
613	1.06	1.11	1.25	1.25	1.38
614	1.01	0.98	0.98	1.02	1.16
810	1.68	1.70	1.62	1.55	1.54
811	1.54	1.52	1.50	1.37	1.27
812	3.00	2.88	2.37	1.45	2.05
813	1.54	1.44	1.35	1.18	1.18
814	1.70	1.66	1.60	1.50	1.50
910	1.60	1.72	2.02	2.03	1.51
911	1.62	1.55	1.53	1.56	1.45
912	1.38	1.52	1.62	1.49	1.46
913	1.78	1.68	1.70	1.62	1.33
914	1.80	1.77	1.71	1.59	1.57

120	1.53	1.49	1.31	1.36	1.16
121	1.44	1.47	1.45	1.42	1.42
122	2.56	2.60	2.37	2.32	1.88
123	1.21	1.35	1.38	1.51	1.32
124	1.36	1.39	1.33	1.47	1.49
420	1.23	1.33	1.39	1.48	1.44
421	1.42	1.41	1.51	1.58	1.61
422	1.15	1.74	2.04	2.42	1.85
423	1.23	1.35	1.47	1.32	1.45
424	1.30	1.35	1.35	1.40	1.30
520	1.54	1.71	1.78	1.50	1.17
521	1.59	1.61	1.55	1.56	1.44
522	0.91	0.90	1.00	0.99	0.69
523	1.67	1.63	1.43	1.42	1.31
524	1.42	1.54	1.56	1.60	1.44

TABLE 11

Areas of Maximum Density, by Scene

Scene	Description of Area Where Density Was Recorded
01	Shadow of largest building
11	Shadow of largest building
41	Sea near vicinity of ship bows
51	Most open area of sea in corner of scene
61	Shadow of building
81	Dark area adjacent to third darkest step in stepwedge
91	Largest area of shadow (shadow of building)
12	Shadow of building
42	Open sea in empty corner
52	Open sea in corner opposite stepwedge

Superimposed on the variability due to photographic processing is a number of trends associated with the amount of noise present. For example, if the darkest scene area has signal level 0, then additive noise will result in a skewed Gaussian distribution:

$$p(\bar{\ell}) = 1/(\sigma\sqrt{2\pi}) \exp(-(\ell^2)/(2\sigma^2)). \tag{12}$$

The expected, or mean level $\bar{\ell}$ will be that measured by the densitometer, since it has an integrating effect, i.e.,

$$\bar{\ell} = \left[1/(\sigma\sqrt{2\rho})\right] \int_0^{255} \ell \cdot \exp(-(\ell^2)/(2\sigma^2))\, d\ell, \tag{13}$$

which approximates

$$\bar{\ell} = \left[1/(\sigma\sqrt{2\pi})\right] \sigma^2 = 0.4\sigma. \tag{14}$$

Our four levels of noise give expected values 1, 2, 4, and 8, which typically result in densities of 1.68, 1.60, 1.49, and 1.14 in hardcopy. This reduction of background density with increasing noise is evident in scenes 01, 51, 81, and 91. Interestingly, the airfield scene 61 exhibits the reverse trend. This is due to the high mean brightness (low mean density) apparent in Table 9 and the broad histogram of Figure 20 (e).

VI. DISCUSSION

We have reported our attempts to develop an imagery database from high quality aerial photography relevant to the image interpretation task. Specifically, we have created two versions of a database of 250 images, consisting of 10 scenes each represented at 5 levels of noise.

The digital database is in 8-bit format on 9-track tape with 4096 bytes (pixels)/record and 4096 records/image file. We have achieved, to high accuracy, the specifications for blur and additive noise. The effect of signal-dependent noise caused by the grain in the original photographic transparencies needs to be studied. At present, all data derived from digitization of the transparencies are regarded as "signal", or "ground-truth".

The hardcopy database, on Kodak 2415 film, suffers from a number of drawbacks not seen in the digital version. Problems were encountered in the control of film-playback on the Dicomed and in darkroom repeatability. Nevertheless, these variations are well quantified in this report and the hardcopy database is useful and representative of our operational image quality. In spite of the limitations of the hardcopy imagery, very good PI data were obtained, supporting the notion that errors in the database were small

compared to the main effects of the variables of interest. These results are described in other reports in this series.

The digital database is clearly better controlled than the hardcopy database. We feel that since most of our program will use the digital database in subsequent experiments, then the reduced consistency of hardcopy is not particularly critical.

REFERENCES

Forsythe, G. E., Malcolm, M. A., and Moler, C. B. Computer methods for mathematical computation. Englewood Cliffs, NJ: Prentice-Hall, 1977.

Pratt, W. K. Digital image processing. New York: Wiley and Sons, 1977, p. 290.

Tupper, J. L. "Control of tone reproduction in photographic systems." In Photographic Systems for Engineers, 1966, 156-166.

Zwick, D. and Brothers, D. L. "RMS granularity: Determination of just-noticeable-differences." SMPTE Journal, 1977, 86, 427-430.

Appendix A

NATO IMAGERY INTERPRETABILITY RATING SCALE

The following is an extract from the Image Interpretability Scale published by the NATO Air Standardization Coordinating Committee (ASCC-AIR STD 101/11, 10 July 1978). It is very similar to the heavily employed National Image Interpretability Rating Scale (NIIRS). Rating categories 0 through 3 are not presented, since they represent ground resolved distances poorer than 2.4 m. Such low resolution, according to photointerpreters employed in our studies, is rarely encountered in aerial photographs of tactical utility.

The terms "detection", "recognition", "identification", and "technical analysis" are also defined herein. Each term represent an increasingly demanding task requiring increasing resolution. Hence, "technical analysis", for example, is prevalent in the descriptions of rating categories 8 and 9.

DEFINITIONS

Ground Resolved Distances: Ground resolved distance is the minimum test target element resolved on the ground. With a system that produces a Ground Resolved Distance (GRD) of 0.3 m, the smallest bar of the test target that is

distinguishable has a physical width of 0.15 m. (A tri-bar test target was used to determine GRD and subsequently to calibrate the Imagery Interpretability Rating Scale).

Detection: In imagery interpretation, the discovering of the existence of an object but without recognition of the object.

Recognition: The determination by any means of the friendly or enemy character of the individuality of another, or of objects such as aircraft, ships, tanks, or of a phenomenon such as communications or electronics patterns.

Identification: In imagery interpretation, the discrimination between objects within a particular type or class.

Technical Analysis: The ability to describe precisely a feature, object, or component imaged on film.

Rating Category 4.

* Ground Resolved Distance, 1.2 to 2.5 m. (3.94 to 8.2 ft.) (47.25 to 98 in.)
* Detect rockets and artillery.
* Recognize troop units.
* Recognize aircraft (such as FAGOT/MIDGET when singly deployed).
* Recognize missile sites (SSM/SAM). Distinguish between missile types by the presence and relative position of wings and control fins.
* Recognize nuclear weapons components.

* Recognize land minefields.
* Identify ports and harbors.
* Identify railroad yards and shops.
* Identify trucks at ground force installations as cargo, flatbed, or van.
* Identify a KRESTA by the helicopter platform flush with the fantail, a KRESTA II by the raised helicopter platform (one deck level above fantail and flush with the main deck).

Rating Category 5.

* Ground Resolved Distance, 0.75 to 1.2 m. (2.46 to 3.94 ft.) (29.53 to 47.25 in.)
* Detect the presence of call letters or numbers and alphabetical country designator on the wings of large commercial or cargo aircraft (where alphanumerics are three feet high or greater).
* Recognize command and control headquarters.
* Identify a singly deployed tank at a ground forces installation as light or medium/heavy.
* Perform Technical Analysis on airfield facilities.
* Perform Technical Analysis on urban areas.
* Perform Technical Analysis on terrain.

Rating Category 6.

* Ground Resolved Distance, 40 to 75 cm. (1.31 to 2.46 ft.) (15.75 to 29.5 in.)
* Recognize radio/radar equipment.
* Recognize supply dumps (POL/Ordnance).
* Recognize rockets and artillery.
* Identify bridges.
* Identify troop units.
* Identify coast and landing beaches.
* Identify a FAGOT or MIDGET by canopy configuration when singly deployed.
* Identify the following ground force equipment: T-54/55 tank, BTR-50 armored personnel carrier, 57 mm AA gun.
* Identify by type, RBU installation (e.g., 2500 series), torpedo tubes (e.g., 21 in./53.34 cm), and surface-to-air missile launchers on a KANIN DDG, DRIVAC DDGSP, or KRESTA II.
* Identify a ROMEO-class submarine by the presence of the cowling for the snorkel induction and the snorkel exhaust.
* Identify a WHISKEY-class submarine by the absence of the cowling and exhaust.

Rating Category 7.

* Ground Resolved Distance, 20 to 40 cm. (0.66 to 1.31 ft.) (7.87 to 15.75 in.).
* Identify radar equipment.

* Identify major electronics by type on a KILDEN DDGS or KASHIN DLG.
* Identify command and control headquarters.
* Identify nuclear weapons components.
* Identify land minefields.
* Identify the general configuration of an SSNB/SSGN submarine sail, to include relative placement of bridge periscope(s) and main electronics/navigation and equipment.
* Perform Technical Analysis on ports and harbors.
* Perform Technical Analysis on railroad yards and ships.
* Perform Technical Analysis on roads.

Rating Category 8.

* Ground Resolved Distance, 10 to 20 cm. (0.33 to 0.66 ft.) (3.94 to 7.87 in.)
* Identify supply dumps (POL/Ordnance).
* Identify rockets and artillery.
* Identify aircraft.
* Identify missile sites (SSM/SAM).
* Identify surface ships.
* Identify vehicles.
* Identify surfaced submarines (including components such as ECHO II SSGN sail missile launcher elevator guide and major electronics/navigation equipment by type).
* Identify, on a KRESTA II, the configuration of major components of larger electronics equipment and smaller electronics by type.

* Identify limbs (arms, legs) on an individual.
* Perform Technical Analysis on bridges.
* Perform Technical Analysis on troop units.
* Perform Technical Analysis on coast and landing beaches.

Rating Category 9.

* Ground Resolved Distance, less than 10 cm. (< 0.33 ft.) (< 3.94 in.)
* Identify in detail the configuration of a D-30 howitzer muzzle brake.
* Identify in detail on a KILDEN DDGS the configuration of torpedo tubes and AA gun mountings (including gun details).
* Identify in detail the configuration of an ECHO II SSGN sail including detailed configuration of electronics communications equipment and navigation equipment.
* Perform Technical Analysis on radio/radar equipment.
* Perform Technical Analysis on supply dumps (POL/Ordnance).
* Perform Technical Analysis on rockets and artillery.
* Perform Technical Analysis on missile sites.
* Perform Technical Analysis on nuclear weapons components.

Appendix B

ILLUSTRATION OF DATABASE

For purposes of database demonstration, we use an aerial scene of the U.S. Army Tank and Automotive Command (TACOM), Warren, Michigan. (This scene was not included in the 10 photographs of the database.) The original negative was exposed at an altitude of 1820 ft. with a lens of 6 in. focal length, yielding a scale of 1:3640. Digitization at 20 μm intervals is therefore equivalent to a "ground truth" resolution of approximately 2.9 in. Figure 23 shows this ground truth image, with no additional blur or noise, in a form illustrating only every eighth pixel of every eighth line out of the total of 4096 x 4096 pixels.

As described in the text, we generated the following equivalent GRD values, by means of digital blurring: "ground truth", 15, 30, 61, and 122 cm. Figure 24 illustrates a matrix of nine degraded images, covering an area of 512 x 512 pixels at full resolution, selected from the global scene of Figure 23. We show only three levels of blur (ground truth, 30, and 122 cm) and three levels of noise (nominal SNRs of 200, 50, and 12.5).

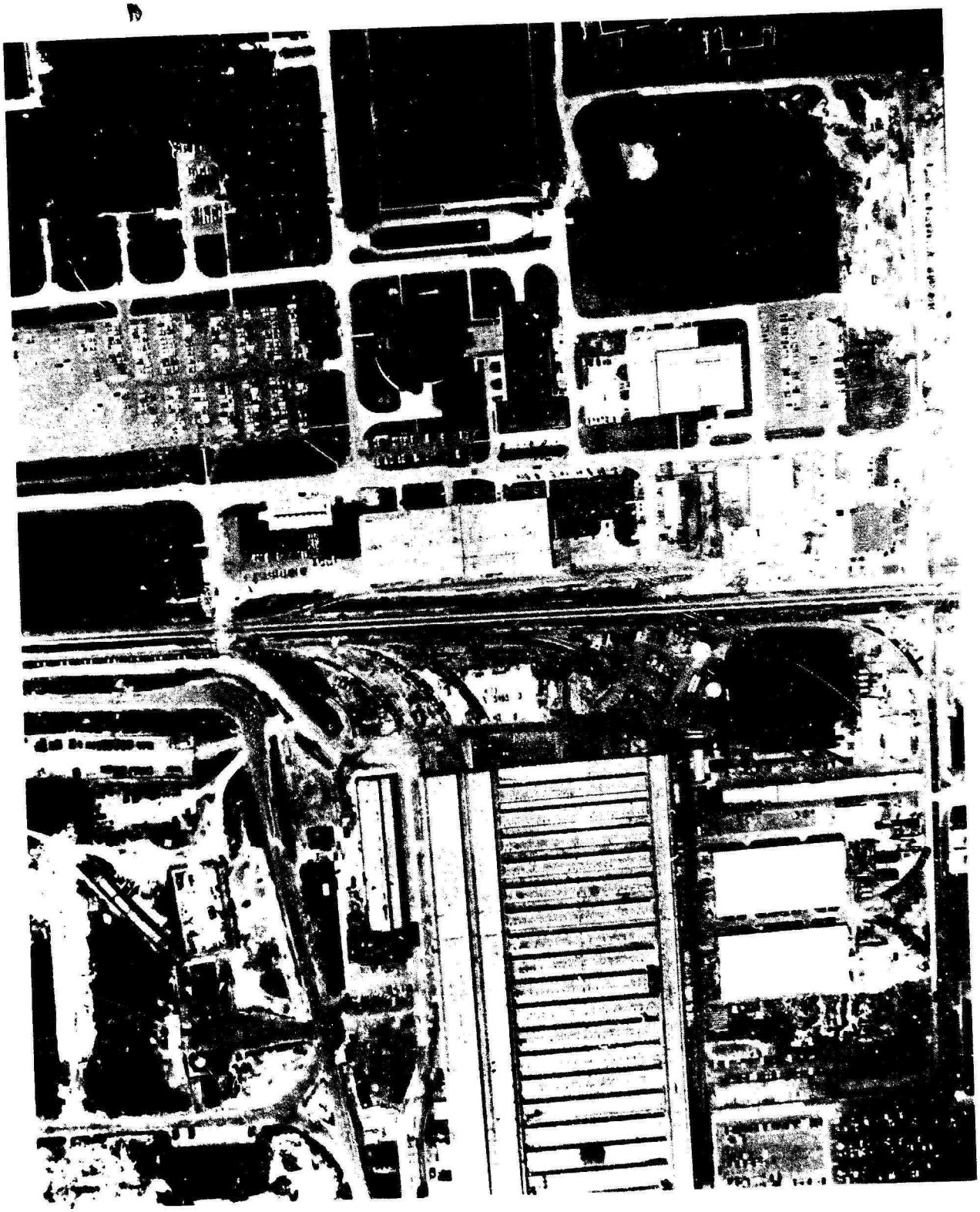

Figure 23: Example of database ground truth, i.e., no additional degradation

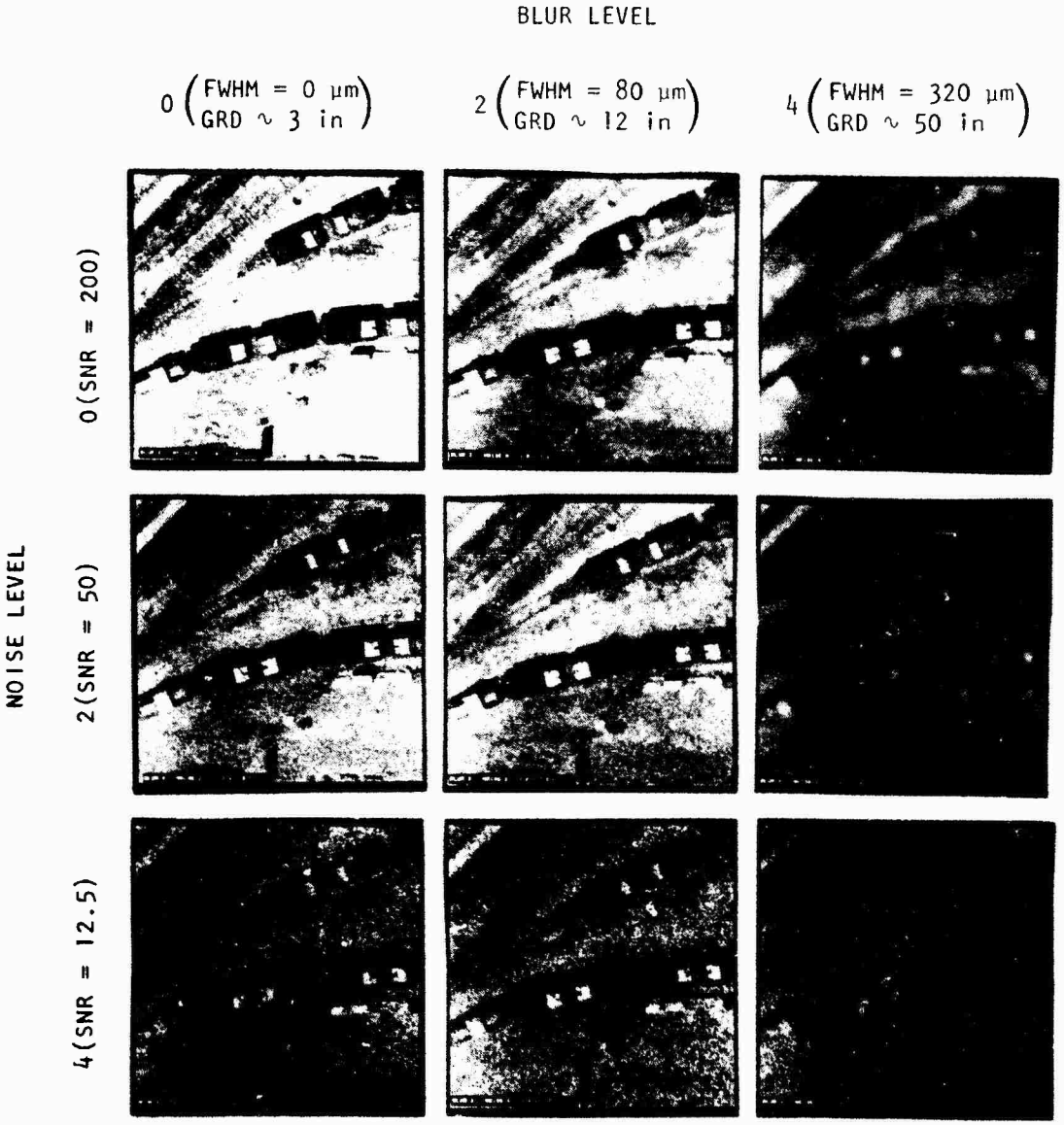

Figure 24: Example of degraded database

Appendix C

SCAN CHARACTERISTICS AND SETUP PROCEDURE FOR THE PDS MICRODENSITOMETER

The original digitized data were prepared by scanning the Precision Photo positive transparencies. The scanning was performed on a PDS Model 1010A microdensitometer. The specifications, as supplied by the manufacturer, are listed in Table 12. Figure 25 shows a rough sketch of the optical system layout for this instrument.

Data were generated by scanning in transmission mode, i.e., $N_{out} = KT$ where K is some constant. The microdensitometer is capable of generating 12 bits of data per pixel. For convenience, the scans were set up so that the maximum transmission reading for a particular scene would yield a digital value of 2000. There are three adjustments to be made when setting up the scans to insure that the data will lie within this range of 0 to 2000. First, the region of the film with the highest transmission is placed in the beam. Then, various neutral density filters are inserted in the beam until a specified photomultiplier tube (PMT) current has been reached. If this PMT current cannot be obtained by changing neutral density filters alone, the filter which comes closest to yielding this specified value is left in the beam. At this

TABLE 12

Specifications of PDS 1010A

PDS	Microdensitometer:	Specifications:
Stage Motion	X and Y travel	254 mm max
	Positioning Accuracy	±1 μm
	Straightness of Travel	±5 μm
Illumination System	Microscope Objective	10X, 0.25 NA
	Microscope Eyepieces	5X, 10X, 15X, 20X
	Apertures	8 Selectable Apertures
Scanning System	Microscope Objective	10X, 0.25 NA
	Microscope Eyepieces	5X, 10X, 15X, 20X
	Apertures	8 Selectable Apertures
	Detector	S11 PMT, 25 mm diameter

stage, the voltage on the PMT dynodes is varied until the desired output current is obtained. Now, two further adjustments need to be made. The voltage generated by the PMT current is amplified before being input to the A/D converter. The gain of this amplifier is adjusted so that the signal input yields a digital value of 2000. Also, the zero level of this differential amplifier must be adjusted so that the dark current of the PMT gives an output value of

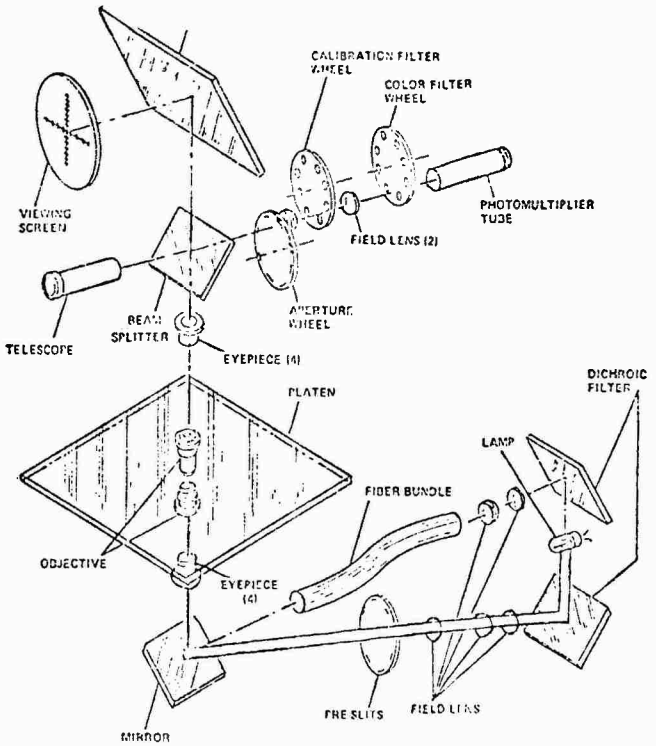

Figure 25: Preslit light path

zero. This is done by blocking the beam with an opaque filter and adjusting the offset voltage of the amplifier. The gain and offset adjustments for the amplfier must be iterated until both conditions, MAX = 200, MIN = 0, are met.

Figure 3 of this report illustrates the relationship between the number output by the A/D converter and the diffuse density of the area being scanned. Although the exact intercept along the log N axis is weakly dependent upon the gain of the amplifier, the only major differences among the curves are their lateral displacement and their nonlinear tails for small values of log N. Over the 8-bit range of interest here, the curves are well approximated by:

$$D = [(D_{min} - D_{max})/\log N_{max})] \log N + D_{max} \qquad (C1)$$

The shape of the nonlinear tail of the log(N) versus $D_{diffuse}$ curve arises as follows. The linear portion of the curve suggests that the scanning geometry of the microdensitometer is such that $T_D = (T_{diffuse})^{1.40}$. (The specific slope depends on the film and the numerical apertures of the densitometer.) Now the current from the PMT consists of a contribution due to the signal, plus a contribution due to dark current, i.e., $I_{PMT} = K_1(T_{dif}^{1.40} + 0_{DC})$ where 0 is the dark current term. This current is converted to a voltage and amplified by a linear differential amplifier before being fed to an A/D converter. Thus,

$$V_{out} = K_2\{(K_1(T_{dif}^{1.40} + 0_{DC}) + V_{off}\}. \quad (C2)$$

Here K_2 is a constant which represents the gain setting of the amplifier, while V_{off} is the reference voltage level which is adjusted so that when only dark current is present, $V_{out} = 0$, i.e., $V_{off} = K_1\ 0_{DC}$.

Since the number recorded by the microdensitometer is proportional to the output voltage, we can see that

$$N_{out} = K'(T_{dif})^{1.40} \quad (K'_{DC} + K_2V_{off}). \quad (C3)$$

If the offset is accurately set,

$$\log N_{out} = \log K'T_{dif}^{1.40}. \quad (C4)$$

If there is some error in the offset setting, then

$$\log N_{out} = \log(K_1 T^{1.40} + \varepsilon). \qquad (C5)$$

Equation (C4) implies that the log N versus D_d is a straight line of slope -1.40. Equation (C5) predicts the same behavior for large values of T_{dif}, provided is small. However, for small T_{dif}, Equation (C5) predicts a tail whose exact shape depends upon the sign and magnitude of ε.

The leftmost curve of Figure 3 illustrates the effect of a (typical) small, negative offset error. The other two curves exhibit the (intentionally produced) effects of larger positive offset errors.

Appendix D

TECHNICAL SPECIFICATIONS MODEL D47 DIGITAL COLOR IMAGE RECORDER

TECHNICAL SPECIFICATIONS

MODEL D47

DIGITAL COLOR IMAGE RECORDER

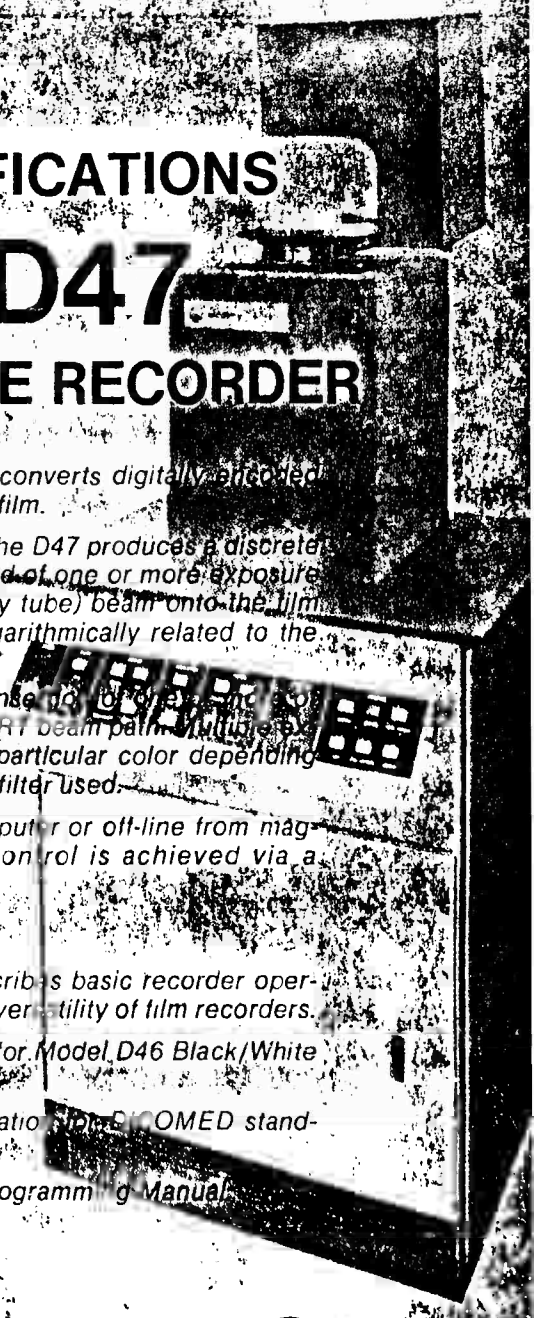

The Model D47 Digital Color Image Recorder converts digitally encoded data to high-resolution color or black and white film.

Each data word (exposure code) transmitted to the D47 produces a discrete picture element (pixel). Each pixel is constructed of one or more exposure spots generated by focusing a CRT (cathode-ray tube) beam onto the film plane. Exposure energy is either linearly or logarithmically related to the data word value.

Color recording is achieved by the sequential insertion of one of three (blue, green & red) spectral filters in the CRT beam path. Multiple exposure through the various filters produces a particular color depending on the relative exposure energy levels for each filter used.

The D47 can operate on-line from a digital computer or off-line from magnetic tape. Operation under full program control is achieved via a 21-command instruction repertoire.

ADDITIONAL REFERENCES

Bulletin 12G123—*Illustrated brochure describes basic recorder operation, overall control flexibility, and plotting versatility of film recorders.*

Bulletin 12D034—*Technical Specifications for Model D46 Black/White Film Recorder.*

Specification #500103—*Technical Specification for DICOMED standard 8-bit parallel TTL interface.*

Technical Manual 12M051—*Operation & Programming Manual.*

DICOMED Corporation

9700 NEWTON AVE. SO. • MINNEAPOLIS, MN. 55431 • (612) 888-1900

BULLETIN 12D035
11/75

DICOMED®

TECHNICAL SPECIFICATIONS

MODEL D47

DIGITAL COLOR IMAGE RECORDER

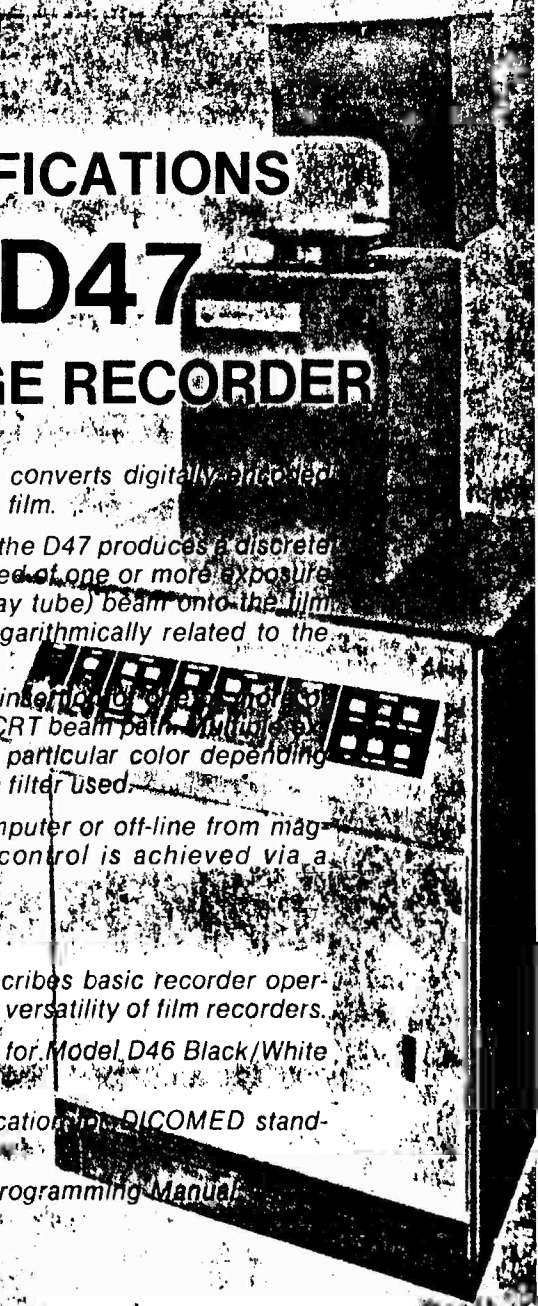

The Model D47 Digital Color Image Recorder converts digitally encoded data to high-resolution color or black and white film.

Each data word (exposure code) transmitted to the D47 produces a discrete picture element (pixel). Each pixel is constructed of one or more exposure spots generated by focusing a CRT (cathode-ray tube) beam onto the film plane. Exposure energy is either linearly or logarithmically related to the data word value.

Color recording is achieved by the sequential interposition of one of three (blue, green & red) spectral filters in the CRT beam path. Multiple exposure through the various filters produces a particular color depending on the relative exposure energy levels for each filter used.

The D47 can operate on-line from a digital computer or off-line from magnetic tape. Operation under full program control is achieved via a 21-command instruction repertoire.

ADDITIONAL REFERENCES

Bulletin 12G123—*Illustrated brochure describes basic recorder operation, overall control flexibility, and plotting versatility of film recorders.*

Bulletin 12D034—*Technical Specifications for Model D46 Black/White Film Recorder.*

Specification #500103—*Technical Specifications for DICOMED standard 8-bit parallel TTL interface.*

Technical Manual 12M051—*Operation & Programming Manual.*

DICOMED Corporation

9700 NEWTON AVE. SO. • MINNEAPOLIS, MN. 55431 • (612) 888-1900

BULLETIN 12D035
1/75

DICOMED®

GEOMETRIC PERFORMANCE

The geometric specifications shown below cover three different film formats as well as two different CRT configurations; high resolution CRT (standard) and ultra-high resolution CRT (optional).

EFFECTIVE RECORDING AREA:
70mm Film Format: 54mm x 54mm maximum
105mm Film Format: 97mm x 97mm maximum
4" x 5" Film Format: 86mm x 86mm maximum

PIXEL CONSTRUCTION: Each picture element (pixel) is constructed by one or more CRT spot exposures depending on the plotting resolution selection (see figure).

High Resolution: 1 spot per pixel.
Medium Resolution: 4 spots per pixel.
Low Resolution: 16 spots per pixel.

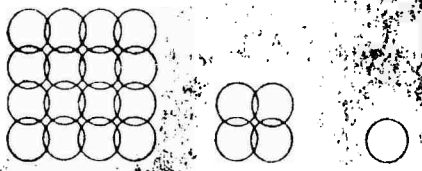

PIXEL CONSTRUCTION FOR LOW MEDIUM AND HIGH PLOTTING RESOLUTION. SPOT SIZE IS CONSTANT.

PLOTTING MATRIX: Each D47 offers push-button or program selection of three different plotting matrices yielding three different resolutions.

	STANDARD CRT	OPTIONAL CRT
Low Resolution	512 x 512 pixels	1024 x 1024 pixels
Medium Resolution	1024 x 1024 pixels	2048 x 2048 pixels
High Resolution	2048 x 2048 pixels	4096 x 4096 pixels

RESOLUTION: Standard High Resolution CRT: 2000 resolvable lines. Optional Ultra-high Resolution CRT: 3000 resolvable lines.
NOTE: Resolution measured on Plus X Pan 4147 film.

GEOMETRIC ACCURACY: "Percent" specifications are referenced to the major axis (H_c or V_c) of the recording matrix. Refer to the figure below for definitions of recording matrix measurements.

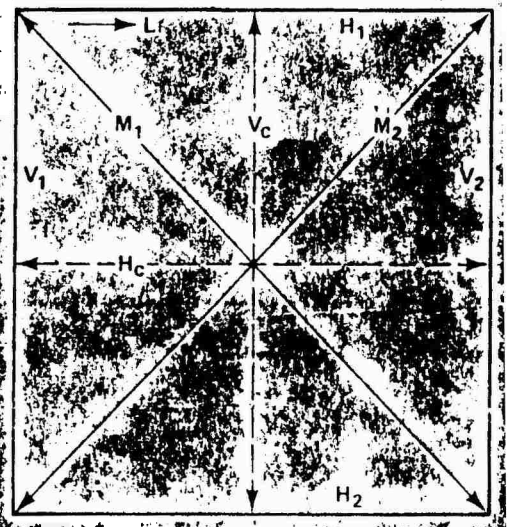

PLOTTING MATRIX MEASUREMENT DEFINITIONS

ARRAY GEOMETRICS

H_1 = Length of top horizontal line
H_c = Length of horizontal major axis
H_2 = Length of bottom horizontal line
V_1 = Length of left vertical line
V_c = Length of vertical major axis
V_2 = Length of right vertical line
M_1 = Length of 0,0 to max., max. matrix diagonal
M_2 = Length of 0, max. to max., 0 matrix diagonal
L = Direction of scan line

Matrix Orthogonality (0): ±0.25% max.

$$0 = \pm\left(\frac{M_1 - M_2}{M_1 + M_2}\right) \times 100$$

Matrix Rectangularity (R): ±0.3% max.

$$R = \pm\left(\frac{H_c - V_c}{H_c + V_c}\right) \times 100$$

Line Curvature (P); (pin cushion distortion): ±0.15% max.

$$P = \pm\left(\frac{d}{H_c}\right) \times 100 \text{ or } P = \pm\left(\frac{d}{V_c}\right) \times 100$$

d = Maximum deviation from best fit straight line.

Spacial Repeatability (S): ±0.05% max.

$$S = \pm\left(\frac{d}{H_c}\right) \times 100 \text{ or } S = \pm\left(\frac{d}{V_c}\right) \times 100$$

d = Maximum displacement of any given point for successive images repeated during a 20-minute interval.

Point Spacing Linearity (L): ± 0.35% Max.

$$L_H = \pm\frac{S_{Hmax} - S_{Hmin}}{2H_d} \times 100; \; L_V = \pm\frac{S_{Vmax} - S_{Vmin}}{2V_c} \times 100$$

Smax and Smin are the maximum and minimum resultant line segments constructed from an internally generated test pattern. The pattern divides each major axis into eight segments.

Trapezoiding (T): ± 0.3% max.

$$T_H = \pm\left[\frac{H_1 - H_2}{H_1 + H_2}\right] \times 100$$

$$T_V = \pm\left[\frac{V_1 - V_2}{V_1 + V_2}\right] \times 100$$

RECOMMENDED FILM TYPES

FILM USE	FORMAT	FILM TYPE
Positive Color Transparency	4" x 5" sheet	Kodak Ektachrome 6115
Positive Color Transparency	70mm, 105mm roll	Kodak Ektachrome MS Aerographic 2448
Black/White Transparency	4" x 5" sheet	Kodak Super-XX 4142
Black/White Transparency	4" x 5" sheet	Kodak Plus X Pan 4147
Color Print	4" x 5" sheet	Polaroid Type 58
Black/White Print	4" x 5" sheet	Polaroid Type 52
Black/White Print & Transparency	4" x 5" sheet	Polaroid Type 55

PHOTOMETRIC PERFORMANCE

The D47 is capable of converting an exposure code into any one of 64 exposure levels (6-bit code) or 256 exposure levels (8-bit code). The constant intensity CRT beam is time-modulated to produce exposures either linearly or logarithmically related to the exposure code.

EXPOSURE RANGE: Depends on film type; range is 2.0D (diffuse Density units) for Ektachrome 6115 film and 1.8D for Plus X Pan 4147 film.

EXPOSURE UNIFORMITY: Uniformity of exposure over the entire plotting matrix is expressed in diffuse density units (D) deviation assuming a film gamma = 1. Specifications are given for units with and without an optional High-Uniformity Module (HUM).

STANDARD UNIFORMITY: ±0.075D max.
UNIFORMITY WITH HUM: ±0.035D max.

EXPOSURE CONTROL: The CRT beam intensity may be varied to compensate for different film speeds. Note: The exposure level may be periodically checked and recalibrated by use of the digital panel meter on the TEST and CALIBRATION panel.

RECORDING SPEED

The total time required to record an image is a function of (1) plotting matrix size (number of CRT spots), (2) the average exposure level required, and (3) the number of filters selected. The time required to record any given pixel is a function of (1) number of spots per pixel and (2) the exposure level required.

SPOT EXPOSURE TIME: 7μ sec. average code; 30 sec. max. NOTE: times are for recording in log mode.

I/O TIME: 2μ sec. max.

ADJACENT SPOT POSITIONING TIME: 8μ sec. max.

RANDOM POSITIONING TIME: 1.0 msec. per axis

FLYBACK TIME: 1.0 msec.

IMAGE GENERATION TIME: The following times are those required for recording the full matrix in log mode utilizing average codes.

Standard CRT: 1.5 minutes in black/white; 4.5 minutes in full color.

Optional CRT: 5.5 minutes in black/white; 16.5 minutes in full color.

COLOR SYSTEM

Full color recording is achieved by sequentially exposing the film through a series of compensated spectral filters. The entire image is first exposed through one filter and the next filter is rotated into position (program or push-button commanded) for the next exposure. A blank position is provided for black/white recording.

BLUE FILTER:	Wratten #47
GREEN FILTER:	Wratten #58B
RED FILTER:	Wratten #25
CRT PHOSPHOR:	P48

OPERATING & TEST PANELS

The recorder includes an operations control panel and a test (and calibration) panel. Items on the test panel are indicated by.*

POWER: Key operated OFF, ON & LOCK-ON positions with power indicator.

INPUT: 6-BIT or 8-BIT exposure code push-button selection.

OUTPUT: NORMAL or COMPLEMENT data polarity selection, and LINEAR or LOG code to exposure transfer characteristic selection.

RESOLUTION: Push-button selection of High, Medium, or Low.

EXPOSURE: 10-turn locking type dial for CRT beam intensity adjustment

CONTROL: OPERATE or TEST mode selection: END FILM and FILM ADVANCE indicators (disconnected for sheet film models). RECORD push button for initiating test pattern or image exposure.

FILTER: Push-button selection of NEUTRAL, RED, BLUE or GREEN filter.

TEST & CALIBRATION METER(*): 000.0 to ±199.9 D digital panel meter for monitoring exposure calibration ar various switch-selected (and probed) test points with the recorder.

HIGH-VOLTAGE SWITCH(*): enables high-voltage pow supply to be switched off for safety during internal mai tenance.

TEST SELECT SWITCHES(*): two 12-position select switches select various test voltages and currents with the recorder.

PRIME MODE SWITCH(*): enables CRT to be primed minimize image retention.

Appendix E

ADDITIVE NOISE PRODUCED BY FIIM RECORDER

The first nine steps of a typical SO-015 duplicate (#1102) were scanned with the Kitt Peak National Observatory (KPNO) microdensitometer (10 μm aperture at the film, 50X magnification, matched 0.25 numerical aperture objectives). Table 3 lists, for each step, the diffuse density, D_d, measured with a Macbeth densitometer, a number, N_{KPNO}, proportional to the mean (specular) transmittance recorded by the microdensitometer and a number $_N$ proportional to the root mean square fluctuation in transmittance. The final entry, N_{in}, is the input number to the look-up table for that step. From these data we deduce that

$$\log N_{KPNO} \quad 3.68 - 1.12\ D_d^{(SO-015)}, \tag{E1}$$

and

$$\log N_{KPNO} = 1.68 + 0.85 \log N_{in},\ 1 \leq N_{in} \leq 110. \tag{E2}$$

Equation (E2) somewhat overestimates the measured values of $\log N_{KPNO}$ for the first step (by 0.05). This discrepancy apparently arises from the mismatch of the IUT and the actual 2415-015 processing, which produced a somewhat greater slope than anticipated for small values of N_{in}. We

greater slope than anticipated for small values of N_{in}. We use an average of the six steps (3 through 8) to determine σ_n, with the aid of Eq. (E2) and (E3) below:

$$N_{in}/\sigma N_{in} = (0.4343/\sigma D_{out})\ (d(D_{out}))/(d(\log N_{in}))$$

$$= (N_{KPNO}/\sigma N_{KPNO})\ (d(\log N_{KPNO})/d(\log N_{in})). \qquad (E3)$$

Eq. (E3) makes use of the fact that $\Delta D_{out}/\sigma D_{out}$ is independent of the instrument used to measure density and density fluctuations (whether diffuse or specular), and that N_{KPNO} is proportional to the (specular) transmission of the wedge. Thus, with Eq. (E2) and (E3) and the entries of Table 13, we generate the following values of σ_N for steps 3 through 8:

TABLE 13

Dicomed Noise (σ_N) versus Input Number (N_{in})

Step #	D	N_{in}	$\frac{N_{KPNO}}{\sigma N_{KPNO}}$	σN
3	0.65	34	12.59	3.18
4	0.50	51	17.88	3.36
5	0.41	68	23.64	3.39
6	0.33	85	30.63	3.27
7	0.26	102	35.89	3.34
8	0.21	119	40.27	3.47

From these entries we find

$$\langle \sigma_N \rangle = 3.33, \quad \langle (\sigma_N - \langle \sigma_N \rangle)^2 \rangle = 0.10 \qquad (E4)$$

We conclude that an additive, uniform, uncorrelated contribution to the input noise is an excellent characterization of the Dicomed noise. Its rms value is 3.33 on an 8-bit scale.

The actual input SNR for the hardcopy is accordingly reduced as indicated in Table 14.

TABLE 14

Input SNR for Hardcopy

Noise Level	SNR_{in} - Normal	SNR_{in} - Hardcopy
0	200	75.1
1	100	60.0
2	50	41.6
3	25	23.7
4	12.5	12.3

Appendix F

PHOTOGRAPHIC PROCESSING FOR HARDCOPY

The maximum densities measured from the Precision Photo originals are listed in Table 15.

TABLE 15

Maximum Densities in Original Photo, by Scene

Scene	Density	Scene	Density
01	2.1	81	1.8
11	1.8	91	1.8
41	1.7	12	1.9
51	2.1	42	1.7
61	1.7	52	2.0

We intended that the maximum density of our final hardcopy ($D_{out_{max}}$) be approximately 1.8, this being the average value of the Precision Photo originals which we wished to emulate. Experience in 2415/SO-015 contact printing and Dektol processing warned us that the post-Dicomed hardcopy originating from the darkroom at USC would have to be no higher in density than around 1.6. We also

learned that we could successfully "contrast stretch" maximum densities between 1.3 and 1.6 to our goal of 1.8 by careful Dektol processing; however, Dicomed playbacks darker than 1.6 inevitably resulted in higher SO-015 densities. Calibration was achieved by contact-printing (30 second exposure) a Kodak stepwedge onto SO-015, which was then developed in Dektol at 68°F for times ranging from 2 to 7 minutes. Calibration data are illustrated in Figure 26. We next drew curves of input density against development time to yield constant output density, and calculated a correction for the contact exposure time in order to shift the actual maximum 2415 density to a suitable value in the abscissa. This latter constraint was designed to give development times and shifts of relative input density which would produce, as near as possible, linear 2415/SO-015 tonal transfer curves.

Table 16 lists the results of the final maximum hardcopy stepwedge densities. Our early attempts to accommodate the variability of the Dicomed-2415 output are reflected in the relatively high values of mean and standard deviation within each scene for blur levels 2 and 0. (Although stepwedge data are not available for blur level 2 images, we were able to estimate the maximum density from comparisons with trends in other blur levels.) Contributing to the improved processing was our realization of the need to adjust the exposure time during contact printing for each transparency,

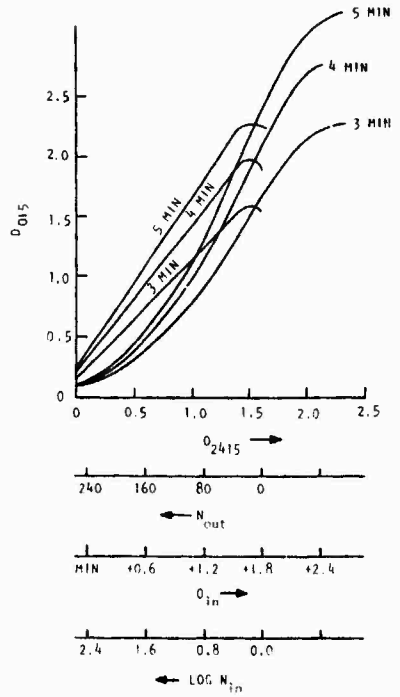

Figure 26: Characteristic curves for S0-015 film developed in Dektol.

The derivative of the characteristic of each curve is also illustrated. The approximate (ideal) relationship between D and the quantities of Figure 17 is illustrated by the additional three scales.

instead of working with batches at constant exposures, thereby allowing the 2415 variability to be compensated by the printing and development. The densities of Table 16 are average values for the set of five duplicates that were produced; the variability over these copies was similar to that shown within the five noise levels.

TABLE 16

Maximum Hardcopy Stepwedge Densities

	Noise Level							
	0	1	2	3	4	Mean	Std. Dev.	Ideal (design)
010	1.85	2.23	1.83	1.59	1.76	1.85	0.23	
011	1.81	1.80	1.76	1.75	1.73	1.74	0.03	
012	1.85	1.44	1.67	1.80	2.00	1.75	0.21	1.8
013	1.73	1.78	1.75	1.75	1.76	1.75	0.02	
014	1.83	1.82	1.83	1.88	1.87	1.85	0.03	
110	2.26	2.35	2.38	2.26	1.77	2.20	0.25	
111	1.81	1.82	1.74	1.74	1.77	1.78	0.04	
112	2.20	2.25	2.28	2.40	2.24	2.27	0.08	1.8
113	1.64	1.65	1.71	1.79	1.69	1.70	0.06	
114	1.82	1.81	1.82	1.84	1.82	1.82	0.01	
410	2.04	2.54	1.75	1.82	1.98	2.03	0.31	
411	1.91	1.92	1.94	1.88	1.98	1.93	0.04	
412	2.25	2.00	1.80	2.00	2.00	2.01	0.16	2.1
413	1.82	1.86	1.85	1.82	1.75	1.82	0.04	
414	1.80	1.79	1.78	1.87	1.77	1.79	0.02	
510	1.86	2.03	2.00	1.93	1.56	1.88	0.19	
511	1.73	1.70	1.70	1.69	1.68	1.70	0.02	
512	2.30	2.10	2.50	2.30	2.20	2.28	0.15	1.8
513	1.77	1.75	1.72	1.73	1.70	1.73	0.03	
514	1.81	1.77	1.77	1.76	1.77	1.78	0.02	
610	1.69	1.83	1.83	1.99	1.91	1.85	0.11	
611	2.04	2.01	2.01	2.06	1.99	2.02	0.03	
612	2.30	2.58	2.12	1.75	2.10	2.17	0.30	2.1
613	2.03	2.02	2.04	2.05	2.00	2.03	0.02	
614	1.82	1.83	1.87	1.86	1.86	1.85	0.02	
810	2.03	1.91	1.90	1.83	1.90	1.91	0.07	
811	1.66	1.66	1.66	1.62	1.61	1.64	0.02	
812	3.10	2.98	2.47	1.55	2.15	2.45	0.63	1.8
813	1.68	1.70	1.67	1.64	1.69	1.68	0.02	
814	1.79	1.78	1.83	1.82	1.84	1.81	0.03	
910	1.90	1.82	2.20	2.23	1.80	1.99	0.21	
911	1.67	1.60	1.61	1.65	1.65	1.65	0.03	

912	1.50	1.70	1.80	1.85	1.80	1.73	0.14	1.8
913	1.74	1.67	1.70	1.76	1.69	1.71	0.04	
914	1.85	1.82	1.84	1.81	1.81	1.83	0.02	
120	2.03	1.89	1.74	1.78	1.75	1.84	0.12	
121	1.60	1.66	1.65	1.64	1.71	1.65	0.04	
122	2.96	3.00	2.47	2.72	2.28	2.69	0.32	1.8
123	1.75	1.77	1.73	1.75	1.70	1.74	0.03	
124	1.88	1.88	1.88	1.86	1.88	1.88	0.01	
420	1.82	1.90	1.96	1.97	1.78	1.89	0.08	
421	1.86	1.89	1.91	1.94	1.89	1.90	0.03	
422	1.65	2.25	2.55	2.80	2.35	2.32	0.43	1.95
423	1.92	1.91	2.01	1.96	1.93	1.95	0.04	
424	1.82	1.82	1.87	1.79	1.82	1.80	0.02	
520	1.89	1.93	2.32	1.97	1.60	1.94	0.26	
521	1.76	1.74	1.79	1.73	1.76	1.76	0.02	
522	1.10	1.10	1.20	1.20	0.90	1.10	0.12	1.8
523	1.78	1.80	1.73	1.77	1.75	1.77	0.03	
524	1.78	1.76	1.75	1.74	1.75	1.76	0.01	

We decided at the time of processing to stretch the stepwedge dynamic range of scenes 41, 42, and 61 beyond 1.8. This was prompted by their broader histograms (particularly scene 41) as evidenced in the lighter appearance of the scenes.

Over the range of input densities in 2415 between 0.0 and 1.5, the three calibration curves of Figure 1 are accurately described as

$$D_{015} = a + b\, D_{2415} + c\, D^2_{2415} \qquad \text{(F1)}$$

where a, b, and c are taken from Table 17 according to the appropriate development time, t_D.

The three additional scales parallel to the D_{2415} scale in Figure 26 illustrate approximately the relations among

TABLE 17

Coefficients for Each Development Time

t_D(min)	a	b	c
3	0.10	0.16	0.51
4	0.11	0.20	0.66
5	0.13	0.25	0.74

the values of D_{in}, the density of the Precision Photo originals, log N_{in}, the log of the corresponding digital value recorded by the microdensitometer (truncated to 8 bits), and N_{out}, the number presented to the Dicomed recorder. The weakest approximation is that between N_{out} and D_{2415}. The N_{out} range was randomly stretched and compressed, with respect to the D_{2415} scale in the hand-processing of the 2415 sheets at USC. The reason for this variability is apparent from a study of Figure 27, taken from a Kodak data release. The characteristic curves of 2415 film (then called SO-115) are extremely sensitive to small changes in development conditions. These curves illustrate changes with development time. Temperature changes would be equally dramatic, as would agitation conditions.

We asked USC to work toward a maximum 2415 density of 1.6 in the step of the wedge corresponding to $N_{out} = 0$, but to

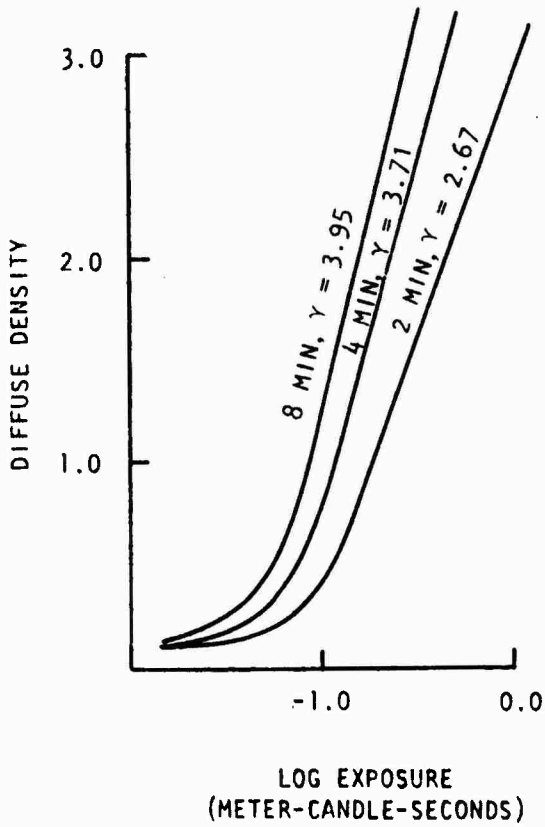

Figure 27: Characteristic curves for Kodak Technical Pan 2415 Developed in Kodak D-19 at 68°F developed in Kodak D-19 at 68° F

err when necessary (it was) toward underdevelopment. As Figure 26 illustrates, such errors could be compensated by reducing the exposure of the 015 copies and increasing their development time. Both actions would increase the slope of the D_{015} versus D_{2415} curve for the actual 2415 record, though generally not enough to compensate for the reduced contrast in the highlights attendant to underdevelopment of the 2415 sheets.